INVESTIGATION OF LASER-BASED SURFACE COATING/ALLOYING OF STEEL SUBSTRATES USING HARD CARBIDES

A Thesis

by

MICHAEL TAYLOR HURST

Submitted to the Office of Graduate and Professional Studies of
Texas A&M University
in partial fulfillment of the requirements for the degree of

MASTER OF SCIENCE

Chair of Committee,	Mathew Kuttolamadom
Committee Members,	Jyhwen Wang
	Chao Ma
Head of Department,	Jorge Leon

December 2020

Major Subject: Engineering Technology

ABSTRACT

The objective of this project is to investigate the coating/alloying of steel surfaces with a hard carbide to improve hardness and wear resistance, with application to metal forming dies. A laser-based additive manufacturing approach, viz., a derivative of selective laser melting (SLM) was used to bond WC-17Co powder on stainless steel and H13 tool steel substrates. An experimental design was created to investigate effects of volumetric energy density (VED) based process parameters on the integrity and properties of the resulting surfaces via microscopy, interferometry, spectroscopy and hardness measurements. Results show up to a 400%+ increase in the surface hardness. With an increasing VED, cracking, spatter, and %W on the surface reduced, while W was detected deeper into the surface, suggesting that an alloying mechanism was gaining dominance. These were further correlated with the differences due to substrates (stainless vs. H13 tool steel) and the original surface characteristics (lapped vs. machined), thus enabling this approach for the coating/alloying of metal forming dies.

ACKNOWLEDGEMENTS

I would like to thank my committee chair, Dr. Kuttolamadom, and my committee members, Dr. Wang, and Dr. Ma for their guidance and support throughout the course of this research. I would also like to thank the head of the department, Dr. Leon, for all of his support during my time in this program.

Thanks also go to my friends and colleagues and the department faculty and staff for making my time at Texas A&M University a great experience.

Finally, thanks to my family for their encouragement throughout this process.

CONTRIBUTORS AND FUNDING SOURCES

Contributors

This work was supervised by a thesis committee consisting of Professor Mathew Kuttolamadom, Professor Jyhwen Wang, and Professor Chao Ma of the Department of Engineering Technology and Industrial Distribution. The equipment used to analyze the elemental concentration and distributions in Chapter 6 was provided by Dr. Paramore and Dr. Butler of the Department of Materials Science and Engineering

Individuals who also aided in contributions to my thesis include Mr. Ming and Mr. Jianchi. Both assisted in the training and operation of the laser.

All other work conducted for the thesis was completed by the student independently.

Funding Sources

Graduate study was supported by Professor Mathew Kuttolamadom from Texas A&M University.

NOMENCLATURE

CVD	Chemical Vapor Deposition
E	Energy density
h	Hatch spacing
LG	Laser Glazing
LSA	Laser Surface Alloying
P	Power
p	Point spacing
PVD	Physical Vapor Deposition
SLM	Selective Laser Melting
t	Exposure time
T	Layer thickness
VED	Volumetric Energy Density
WC-Co	Tungsten carbide-cobalt

TABLE OF CONTENTS

Page

LIST OF FIGURES AND GRAPHS

Page

LIST OF TABLES

1. INTRODUCTION

With a demand for metal tooling to have increased performance and life, such as in the automotive industry, there is a need for a low cost but highly effective means to improve and repair costly metal forming dies. Many metal forming dies and tooling components today are made of tool steels, such as H13. Properties such as hardness and wear resistance determine the capability and longevity of the metal forming tool. With metal forming tools, a significant amount of force/pressure is applied to the tool during the metal forming operation. During this process, a significant amount of heat leads to the degradation of the surface of the metal forming tool. Tools eventually reach their limit in useful tool life and begin to show signs of tooling failure. Common causes of tooling failure consist of cracking, denting, plastic deformation, edge deterioration, wear, and heat checks [1].

Conventional surface improving processes such as Physical Vapor Deposition (PVD), Chemical Vapor Deposition (CVD) have been utilized for years to increase surface hardness and wear resistance of metal forming dies. However, these forms of coating are unable to provide sufficient protection, customizable surface improvement, or repairing capabilities [2]. Both PVD and CVD coatings are very expensive and require a large lead time due to the machinery set up required.

With limitations to conventional coating methods, laser-based surface improvement has been recognized as a potential means of surface coating while improving on the limitations seen in conventional means of surface improvement.

Selective Laser Melting (SLM), will be the laser-based process of choice for conducting experiments. Tungsten carbide-cobalt (WC-Co) powder will be the powder media used for sintering onto the H13 tool steel substrate. Tungsten Carbide-Cobalt is strategically chosen, because cemented carbides consist of a carbide phase that provides excellent wear resistance and a binder phase that provides toughness and ductility [3]. Having these characteristics, the carbide powder material is an excellent candidate to coat a metal forming die where these characteristics are some of the most influential to the metal forming process. H13 tool steel is selected as the substrate as this material is one of the most commonly used in industry for metal forming dies and tools. Using these materials, a selected design of experiments will be developed to investigate the feasibility of coating H13 with WC-Co powder.

2. BACKGROUND AND LITERATURE REVIEW

2.1. Conventional Methods of Coating Metal Forming Dies

Many metal forming tooling pieces today are coated using conventional coating methods that have been the common practice for years. These conventional methods include Physical Vapor Deposition (PVD), Chemical Vapor Deposition (CVD), thermal spraying, ion implantation and ion-assisted coatings. However, these conventional forms of surface coating to improve tool life of metal forming dies are unable to provide sufficient protection, customizable surface improvement, or repairing capabilities [2]. PVD coatings are thin coatings bonded by a mechanical bond. This mechanical bond produces high residual stress which can lead to delamination. PVD coatings (sputtering, vacuum evaporation, and ion plating) are too thin and promote heat checking through crack initiation at the interface between the coating and substrate [2]. CVD requires long preparation times and polishing of the metal forming die is required which can be expensive or impossible. CVD is a high-temperature process that degrades the heat-treated properties of the die substrate [2]. These coatings also require the whole die to be coated and not a localized amount of the surface area. Customization to the coating characteristics also is unattainable using these conventional methods. Only a uniform coating is able to be applied across the surface of the material being coated [4]. Lead time and cost of coating metal forming dies also becomes another important disadvantage to using these conventional methods. These disadvantages to using the

conventional methods of coating metal forming dies are why laser-based surface improvement has been recognized as potential means of surface treatment and coating.

2.2. Hard Carbide as a Potential Coating Material

Carbide powder is strategically chosen, this is because cemented carbides consist of a carbide phase that provides excellent wear resistance and a binder phase that provides toughness and ductility [5]. Having these characteristics, the carbide powder material is an excellent candidate to coat a metal forming die where these characteristics are some of the most influential to the metal forming process, and greatly impact the tool life of the metal forming die. Powdered, or granular, materials are used for the sintering process of WC-Co. Powder characteristics are essential to the print quality and characteristics. The powder characteristics used by Khmyrov to attain the best print characteristics are the following. The most influential powder characteristic is the powder flowability. Flowability can be measured using one of the six methods that are commonly reported to measure the powder flowability: the angle of repose, compressibility index, flow in a rotating drum, flow through an orifice, shear cell and powder rheometers [5]. When using the powder cohesion forces must be accounted for when using grain sizes less than 50 microns [5]. As the cohesion forces increase the powder spreadability to form a single layer becomes increasingly difficult. The powder materials used in Chaolin Tan's study contained the following characteristics. The raw powder was high purity, plasma spheroidized tungsten (W) powder [6]. A highly spherical powder is desired, to improve the flowability, and promote the wetting

between the melt pool and powder particles [6]. Resulting in an increase in the density of the printed object. For these reasons the carbide powder, Tungsten-Carbide Cobalt 17 (WC-Co17), is chosen as the powder material to use in the following experiments. The WC-Co 17 power consists of spherical power granules ranging from 15-45 micrometers in diameter allowing the powder to have great flowability. Also, the cobalt used in this powder has been chemically bound onto the surface of the powder granules. Providing uniform distribution of the binder phase element within powder material.

2.3. Laser Based Manufacturing Approaches of WC-Co

Laser based printing of WC material onto a substrate produced some interesting results in Dr. Wenping 's study [2]. For 2-micron powder used in the study by Dr. Wenping, the hardness of the surface layer was increased by more than 100%, and as expected there is a decrease in hardness with distance from the surface. However, for 300-nm powder alloyed zones, the hardness depth profile is reversed [2]. Opposite to the hardness increase normally expected in the laser-alloyed zones, the hardness was reduced to 25% of the substrate for the 300-nm powder alloyed zone. Process parameters effects on this are the following. An increase in laser power enhances the continuity of the melting pool resulting in cavities that are closed, and the porosity decreases [2]. A reduction in scanning speed causes an expansion of the melting pool and leads to a significant increase in density [2].

In the literature article, obtaining crack-free WC-Co alloys by selective laser melting [3], the parameters used for printing are the following. The SLM printer

operated with a laser beam of 1.07 microns wavelength and focused spot diameter of 100 microns. While the printing parameters were layer heights of 50 to 100 microns, a laser power varying from 50 to 100 W, scanning speed of 10 to 100 mm/s, and line spacing of 50 microns. This spacing allows for approximately 50% overlap of the scanning tracks. In the experiment conducted by Khmyrov, the probability of delamination increases with increasing layer thickness [3]. In this paper the observed maximum layer thickness able to be used is 100 microns. When using the P = 50W and v = 100mm/s on a single layer of powder the effects of the Co composition is observed. Having a 50/50 ratio of WC to Co displays cracking, and when the ratio of Co is increased to 25/75 no cracking is observed. One major challenge noted in the SLM of WC-Co is the tendency for cracking during the printing process due to the high concentration of carbides. According to Khmyrov, increasing the laser powder does improve the material. However, with this increase in laser power also increased cracking frequency [3]. This is the reason for using Co, to mitigate the chances of cracking.

The printing parameters used in Chaolin Tan's experiment consisted of a laser power ranging from 200-370 W, and the laser scanning speed of 100-400 mm/s [6]. Scanning tracts were also conducted using a 67-degree rotation, zig zag pattern, during the printing. Layer height was 20 microns. During the parameterization of the laser parameters energy loss can be divided into three parts, convective heat loss, radiation heat loss, and heat loss through evaporation [6]. Chalin Tan explains another contributing factor to cracking is the oxidation sensitivity may lower wettability and lead

to the formation of cracks when even the small amounts of oxygen are absorbed by the molten pools [6].

Printing parameters used by Dr. Staden consist of a scanning speed between 100-200 mm/s, and a power between 100-200 J/s. The single layer test samples were analyzed by a microscope and observed three different characteristics. Protrusion formation is the first parameter observed. Samples produced having a high volumetric energy density (VED) experience increased material ejection on the sample surface during processing [7]. This corresponds with having a low hatch spacing. An increase in hatch spacing decreases VED which corresponds to a reduction in protrusion formation [7]. Secondly, the shrinkage on the single layer prints are observed. The samples in this experiment exhibit localized shrinkage near the island edges as well as the sample contours [7]. Shrinkage occurs during the rescanning of a previously scanned area due to the overlap. The rescanned area undergoes a second cycle of thermal expansion, particle rearrangement, and subsequent shrinkage. The shrinkage observed varies depending on the process parameters used. The observable shrinkage increases as scan speed and hatch spacing increases [7]. Shrinkage occurring in the localized areas of the specimens also influences the unwanted formation of porosity within the print. According to Dr Staden, increased hatch spacing positively influences the quality of the tract printed under SLM [7]. Samples with low hatch spacing exhibited defects including pitting as a function of particle evaporation, balling due to low hatch spacing and moderate to high scan speed, and cracking due to low hatch spacing and high power. In conclusion this paper suggests

that parameter combinations of low scan speed, high hatch spacing, and high laser power will result in favorable single layer formation.

2.4. Laser Based Surface Alloying of Metal Forming Dies

Laser glazing (LG), a very thin layer (less than 0.5 mm) is melted and 'self-quenched' at a rapid cooling rate, leading to fine grain structures that contain metastable and supersaturated phases, and increased homogeneity [2]. LG has the objective of producing a smooth Ra value of less than 5 microns, and crack free layers. Laser surface alloying LSA has characteristics similar to those of LG but, in addition, changes the chemical composition of surface layers. The coating material is pre-placed or injected into the molten pool on the substrate, and the laser is then used to melt the coating and a portion of the substrate to form an alloyed zone [2]. LSA's objective, similar to that of LG, is to produce a Ra value less than 15 microns, and contain no defects such as cracks.

2.5. Research Gaps & Motivation

A limited amount of research has been conducted on the printability of carbide powders to form bulk parts using laser based additive manufacturing technologies. Though difficult, using carbide powders in additive manufacturing technologies is possible. Limited research has been conducted to identify the optimal ranges of laser parameters needed to yield the best print characteristics on a layer by layer basis. Also, limited research has been conducted to investigate the SLM process to coat a single layer of carbide powder on top of a metallic substrate to improve the surface hardness.

The main focus of this research will be to investigate coating a metallic substrate with a carbide powder to improve surface characteristics that are desirable for metal forming operations. The coating operation will utilize a laser similar to that of a powder bed fusion additive manufacturing technique to melt the powder onto the surface of the substrate. Specifically, this research will look into the influence of energy density on surface characteristics such as hardness, roughness, and elemental composition. This research will answer the question, if it is possible to leverage additive manufacturing processes to improve surfaces of metallic materials rapidly with a level of customization. In the case of success, there are many applications in which this could greatly benefit industry.

Potential benefits to using this method as opposed to one of the conventional methods includes benefits such as selectively hardening regions of the die, repairing, applying textured surface, rapid turnaround with less preparation and cost requirements. One major unknown in conducting this experimental research is the feasibility to print a single layer of WC-Co 17 powder with sufficient surface property improvement to have a significant impact on the metal forming dies tool life. Also, there is the unknown of the desirable laser power and energy density to apply to produce the optimal print results.

3. RESEARCH METHODOLOGY

The objective of this research is to investigate coating metallic surfaces with WC- Co17 to provide improved surface characteristics. This chapter outlines the research methodology that was used for achieving this objective. In addition to the research questions, this chapter lists their associated tasks, methodology and outputs.

3.1. What is the effect of volumetric energy density imparted on the layer morphology while using a stainless-steel substrate? (RQ1)

The objective of RQ1 is to develop and evaluate a design of experiments that encompasses a large range of parameter values. Allowing the optimization of the parameters to yield higher hardness and uniform coating surface. The tasks, methodology, and outputs for RQ1 are listed below:

Task 1A: Analyzes the resulting elemental distributions as a function of the volumetric energy density.

Task 2A: Analyzes the properties (Vickers Hardness) as a function of the energy density.

Methodology: create a design of experiments that span the design space on both ends of the VED range. A uniform surface on the stainless-steel substrate is produced by lapping the surface. Followed by creating the samples fitting the design of experiments. Print quality is captured through the use of microscopic imaging to analyze the coated area for crack s and spatter. Surface and cross-

sectional elemental distribution is measured by EDS. Vickers hardness is taken and averaged values are calculated for each of the samples.

3.2. How does the initial surface condition of the H13 substrate and the volumetric energy density effect the surface morphology? (RQ2)

The objective of RQ2 is to investigate the influence of initial surface conditions having on the surface morphology. Volumetric energy density also is analyzed for the effects the VED has on different surface conditions. The tasks, methodology, and outputs for RQ1 are listed below:

Task 1A: Prepare two surfaces on the H13 substrate for laser processing. One surface is to be machined, and the second surface is to be lapped.

Task 2A: Create the coating samples and characterize each of the samples.

Methodology: First, prepare the two different surfaces to be used for surface coating, and characterize the two different surfaces preprocessing. Define the narrowed range of VED within the design of experiments. Create the printed samples on each of the two different substrates. Each sample will be analyzed under EDS for surface elemental composition, surface profiling for roughness, Vickers hardness, and optical images. Correlating the results from each type of analysis, and comparing the results yielded from both preprocess surface conditions.

4. MATERIALS AND METHODS

4.1. Substrate and Coating Material

The WC-Co powder selected to be used for this research is a WC-Co 17 powder, containing 83% WC and 17% Co by weight. The size distribution of the powder is between 15 and 30 micrometers in diameter. The WC-Co 17 powder is an industrial grade powder that is manufactured for the use in additive manufacturing processes. Cobalt has been chemically bonded to the surface of the WC spherical powder to improve the powders sinterability. Cobalt acts as a binder to promote better fusion of the particles to the surface of the substrate and each other.

Two different substrates are selected for these experiments. Stainless steel is one substate of choice for the preliminary tests due to material being readily available. Also, stainless steel is a common material used in many applications, and this investigation will determine if this process can be applied to the surfaces of multiple substrates. H13 is the second substrate chosen for this investigation. The reasons for choosing H13 are the following. One, is that H13 is one of the more common materials used in metal forming dies. Also, H13 is already a hard tool steel, and this investigation was performed to determine if it is feasible to greatly increase the surface hardness of a material.

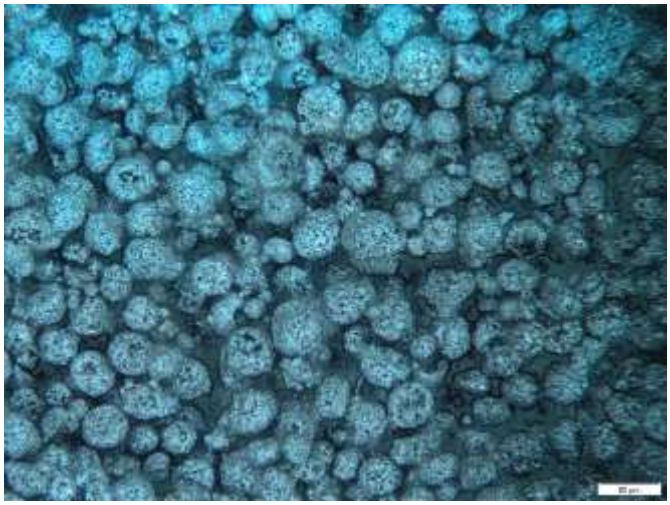

Figure 4-1-1: WC-Co 17 Powder (20X)

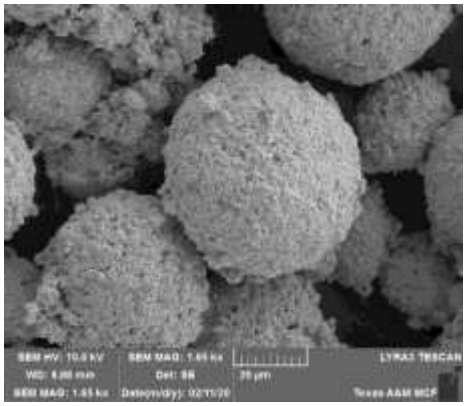

Figure 4-1-2: WC-Co 17 Powder SEM (1.65 kx)

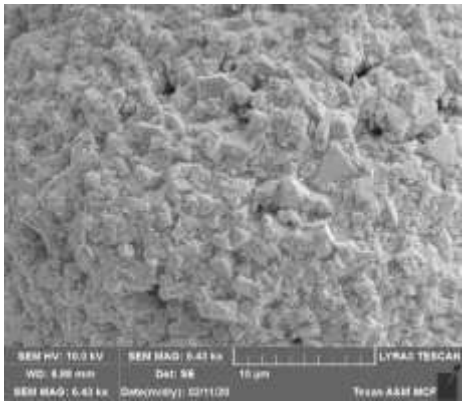

Figure 4-1-3: WC-Co 17 Powder SEM (6.43 kx)

4.2. Design of Experiments

The experimental procedure for this investigation will be to print preliminary samples with energy densities ranging from 200 to 2150 J/mm^3 in increments of 150 J/mm^3 and a power that is set at 200 (W). Both the point and hatch distances are selected to be 0.04mm. These distances are selected to obtain an overlap of approximately 50%, and this follows previous reach done to obtain the highest quality of prints [3]. These

preliminary samples are printed on a stainless-steel substrate instead of the H13. The reason for the preliminary study is to identify a narrower range of energy density to investigate on H13 tool steel. Also, to investigate the feasibility of the research to be conducted on various metallic substrates. Choosing 200(W) is due to the limitations of the laser station, maximum laser power is 200 (W). Resulting in a total of 13 samples needed to account for each of the parameter combinations for stainless-steel (Table 1). Following this experiment, eight energy densities where selected to be applied to the H13 substrate (Table 2). These energy densities have the same parameter values as those used in the preliminary experiment. Each of these eight parameters selected for the H13 substrate will be processed twice. The first will be on a lapped uniform surface on the H13 substrate, and the second with be on a machined surface on the H13 substrate. Exposure time is varying based on the corresponding energy density and power selected. Exposure time (t) is calculated using the following equation, hatch spacing (h), point spacing (p), energy density (E), layer thickness (T), and power (P). There also is a multiplication of 10^{-6} . This is done because for the laser station being used to conduct these experiments exposure time is entered into the print program in microseconds (Equation 1).

$$t = \frac{(h * p * E * T)}{P} * 10^{-6} \quad (1)$$

Based on the size distribution of the powder a layer height of 50.8 micrometers is chosen. This chosen to improve the powders spread ability and to increase the density of the spread powder. Powder spreading is conducted manually with various rollers and

blades over a predetermined area. To establish a confident 50.8 micrometer layer height metal shims are chosen to allow the rollers and blades to move in parallel at a constant height. The print area chosen for the laser to scan is 5mm by 5mm area for conducting the print quality tests. For the printing process a point and hatch distance is chosen to be 0.04mm. These values are chosen based on the laser beams diameter at its focal point being approximately .08mm, and yielding an overlap of approximately 50% of the laser path.

Table 4-2-1: Printing Parameters for Stainless Steel Substrate

Exposure Time (μs)	Energy Density (J/mm^3)
40.6	200
71.1	350
101.6	500
132.0	650
162.5	800
193.0	950
223.5	1100
254.0	1250
284.4	1400
314.9	1550
345.4	1700
375.9	1850
406.4	2000
436.8	2150

Table 4-2-2: Printing Parameters for H13 Tool Steel Substrate

Exposure Time (μs)	Energy Density (J/mm^3)
101.6	500
132.0	650
162.5	800
193.0	950
223.5	1100
254.0	1250
284.4	1400
314.9	1550

4.3. Laser Station

Below is a picture of the laser-based powder bed fusion set up used to conduct these experiments (Fig.4). Argon gas is used as a protective gas in these experiments to decrease the chances of oxidation occurring during the laser sintering process. The scan head, laser generator, and oscilloscope are all of the components for manipulation and monitoring of the laser (Table. 3). The print stage is located where the print chamber is placed for performing the printing process. Also, the print stage can be controlled in the Z direction in order to have the surface of the print to be located at the focal point height of the laser beam from the scan head. Being able to do this allows there to be less energy loss during the printing process.

Finally, the user interface is where the controls for the lasers path are located, and where the user enters the parameters, power and exposure time, used during the

print. For all of these prints the print mode selected is drill mode. In this mode the laser pulses, creating a single pulse located at the point and hatch distances. This mode is selected so that the results attained in this research investigation are relatable to what could be expected from an industrial grade metal printer as well. The other mode that can be selected is the continuous scan where the laser stays on continuously until print layer is complete.

During the procedure a custom vacuum chamber is used (Fig. 5). A vacuum chamber is used in order to have as closed to a controlled environment while the printing process is being conducted. The vacuum chamber used is capable of attaining an O2 level of .002% O2 inside the chamber while performing the experiment. This helps reduce any effects of uncontrollable parameters such as O2 that may cause unintended results of the print quality such as oxidation. We are able to draw conclusions and determine influences of varying parameters without major influence of variables such as O2. Figure 3 shows one of the test runs being printed, and shows what is observed while the printing process in being conducted.

Table 4-3-3: Laser Station Set-Up

1	Laser
2	Laser Generator
3	Scan Head
4	User Interface

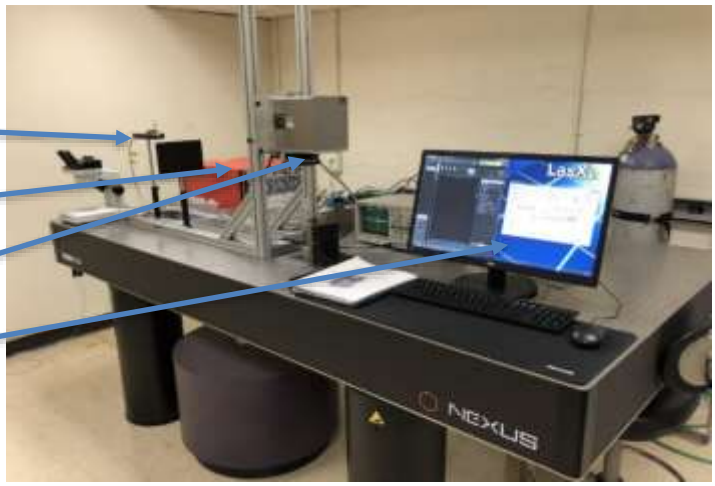

Figure 4-3-4: Laser Station Set-Up

Figure 4-3-5: Laser Station Chamber

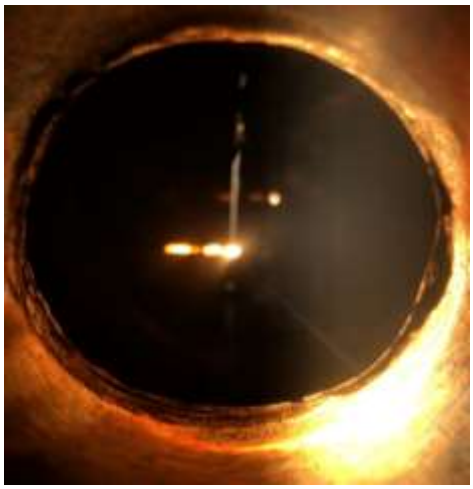

Figure 4-3-6: Live Laser Processing

4.4. Microhardness Testing

The first analysis conducted is a microhardness test. To perform this, test a manual measurement Buhler microhardness testing machine is selected. Setting the

machine to a HV 0.5, 0.5 is the kilogram major load applied, and a 12 second dwell time. These settings were selected due to the fact that the surface of interest when conducting the hardness test is a thin coating. Being a thin coating, to attain data relevant only to the coating means that the hardness penetrator must not penetrate beyond the thickness of the coating. If the penetrator exceeds the coating depth then the substrates hardness will be affecting the results. Penetration depth for Vickers hardness testing is directly correlated with the diagonal measurements, D1 and D2 values, taken to calculate the hardness value [8]. To calculate the estimated depth of penetration the average of the two diagonal values are take, and then divided by seven. Using the HV 0.5 produces a penetration depth ranging from 3-5 micrometers [8]. This allows a significant amount of coating material, coating thickness is approximated 45 micrometers, to remain under the penetration depth to produce accurate results. When testing microhardness on a material one of the expected outcomes is that the data gathered will have a larger standard deviation and variance within the groups. A minimum of ten hardness tests per sample is taken to calculate an average hardness value. Taking ten samples allows the standard deviation and variances within the groups to become less significant. These hardness values are listed in tables, and the corresponding results are plotted on graphs to identify the effects of energy density on hardness.

4.5. Microscopy

Optical imaging is one analysis done to examine the print quality of the print tracts as well as the overall print area, 5mmX5mm for steel and 5mmX10mm for H13.

After printing all of the samples onto the steel and H13 substrates each of the different print samples are observed. To conduct the image testing, an Olympus microscope with monitor display is used to capture the images and take any needed measurements. For the pictures taken there are three different magnifications used 10X, 20X, and 100X. Each of the photos are captured using the bright field setting. The main point of observations is to evaluate cracking and splatter seen to occur on the surface of the coating. For coating metal forming dies the coating needs to be crack free to ensure the integrity of the coating and the coating longevity. Also, when dies are used surface finish of the end product is another important characteristic that is controlled during metal forming. Knowing this, the less splatter seen on the print and increased uniformity in print tracts is needed to produce the best surface finish on the part.

4.6. White Light Interfometer (3D Surface Profiler)

Optical profiling in this investigation of coating on a metal forming die material will be an important point of analysis. The profiler used to capture the surface profiles in this investigation is a ZeGage Pro. ZeGage Pro is a non-contact measurement profiler and allows the characterization of micro-scale features of the coating surface. Having an understanding of the surface characteristics on printed areas within each of the different substrates is imperative. The surface roughness of the coating influences mechanical limitations of the coating, lubrication entrapment, and surface quality of the product being formed. Allowing the coefficient of friction experienced between the interfaces of the die and product to be reduced or manipulated.

4.7. Elemental Analysis

To determine the elemental composition of the coatings an Energy-dispersive X-ray spectroscopy machine is used to examine both the top surface and cross section of the coating. The specific machine used to perform the spectroscopy on the stainless-steel substrate is a Joel JSM-7500F machine. The machine used for the spectroscopy on the H13 substrate is a Phenom XL. Observing the elemental makeup of the coatings provides crucial information to further optimize the coating characteristics through manipulation of the laser parameters. Knowing the elemental composition will further the understanding of what is happening at the melt pool and how the material is reacting to the different energy densities.

5. EFFECT OF VOLUMETRIC ENERGY DENSITY IMPARTED ON THE LAYER MORPHOLOGY ON STAINLESS-STEEL SUBSTRATE (RQ1)

Stainless steel is the substate of choice for the preliminary tests due to material being readily available. Also, stainless steel is a common material used in many applications, and this investigation will determine if this process can be applied to the surfaces of multiple substrates. Allowing the contribution of coating a carbide material with powder bed fusion techniques to be applied to a wide range of materials. Figure four shows the coatings on the stainless-steel substrate, and each of the coated areas measure 5 mm by 5 mm.

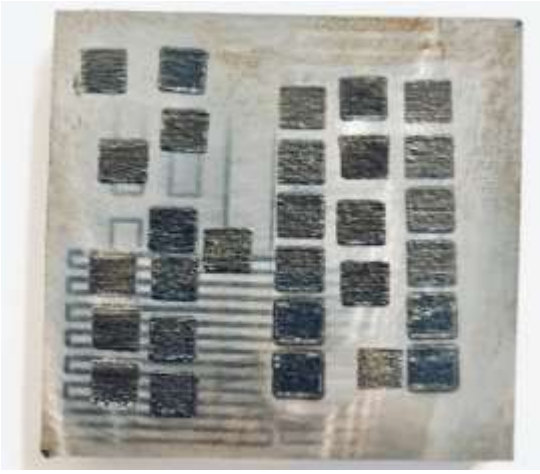

Figure 5-1-1: Stainless-Steel Coatings (5mm by 5mm)

5.1. Optical Images of Stainless-Steel Substrate

Displayed in the figures below, figure 5-2 through figure 5-7, the following observations can be made. In regards to energy density, severe cracking is seen in the lower energy densities, and as energy density increases cracking becomes less prominent. Part of the reasoning behind this crack is first, the material being used is a carbide powder with a binding material. Carbide is a brittle material and when exposed to high thermal shock, rapid heating and cooling, the material can crack easily. Having the severe cracking also can support the reason why the standard deviations of the surface hardness values, stated later in this report, are so high. Cracking can cause the materials hardness value to not be read correctly due to material failure during the loading process in hardness testing. Also, cracking also is a key characteristic of brittle materials which inherently are harder than nonbrittle materials. However, cracking is needed to be minimized to improve the surface quality by lowering surface roughness. With a lower surface roughness metal forming dies and tools will be able to produce a better surface finish on the formed product.

Spatter also decreased in both quantity and size as energy density increased. Decreasing the number of defects located on the surface. Spatter shows that there may not be sufficient amount of energy to bond the WC-Co17 powder to the surface of the substrate before being dislodged from the surface and forming a spatter point. With relation to the laser energy density, print track uniformity improved greatly when increasing the lasers energy density applied to the surface of the substrate.

Figure 5-1-2: Microscope Image 20X (200 J/mm^3) (All scale bars = 50 μm)

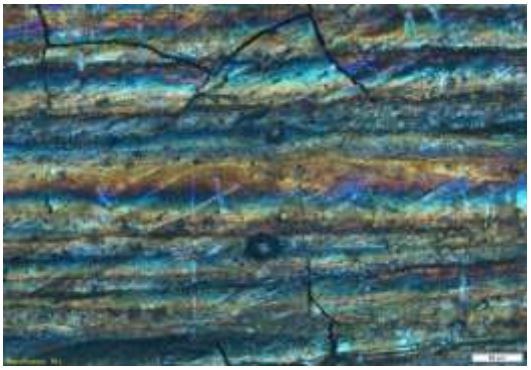

Figure 5-1-3: Microscope Image 20X (500 J/mm^3)

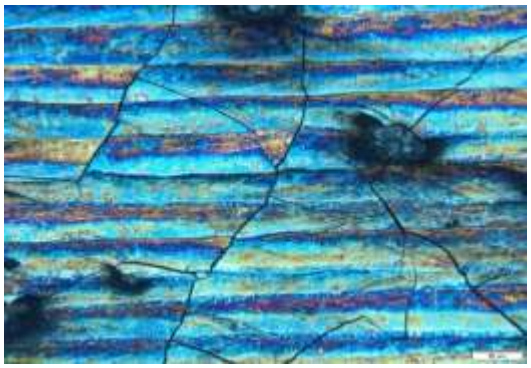

Figure 5-1-4: Microscope Image 20X (800 J/mm^3)

Figure 5-1-5: Microscope Image 20X (950 J/mm^3)

Figure 5-1-6: Microscope Image 20X (1100 J/mm^3)

Figure 5-1-7: Microscope Image 20X (1400 J/mm^3)

5.2. Elemental Composition of Stainless-Steel Substrate

Elemental composition is important to analyze, so the surface and the cross section of the specimens after being exposed to the laser during the laser processing and WC-Co17. Knowing the effects energy density has on the WC-Co 17 powder and the substrate is important to further the understanding of what is happening at the melt pool.

5.2.1. Top Surface of Stainless-Steel Substrate

Observing the top surface of the specimens, the graph bar chart is labeled showing the elements ratios and their compositions seen at the designated energy densities. The objective of this part of the research is to be able to maximize the amount of the W and minimize the amount of Fe located on the surface. A ratio of tungsten to iron atomic concentrations is shown below (Fig. 8). Here there decreasing trend with a drastic decrease in the ratio following the 200 J/mm^3 energy density. A signicicant decline in the ratio is observed through 650 $\boldsymbol{J/mm^3}$. Beyond this energy density the ratio continues to decrease. However, the rate of decline is greatly reduced. Observing this and bar chart (Fig. 9), the amount of W detected on the surface of the specimen is the highest at 200 J/mm^3, equaling 46.43% in weight. The lowest weight percent of W observed in the top surface of a specimens is 6.46% at 1700 J/mm^3. This supports the behavior of the trend in hardness testing, because WC being harder than the substrate of stainless-steel shows that the increase percentage weight of W greatly increases the surface hardness. As the energy density increases in hardness the percentage of Fe increases in weight percent as W decreases causing the reduction in surface hardness.

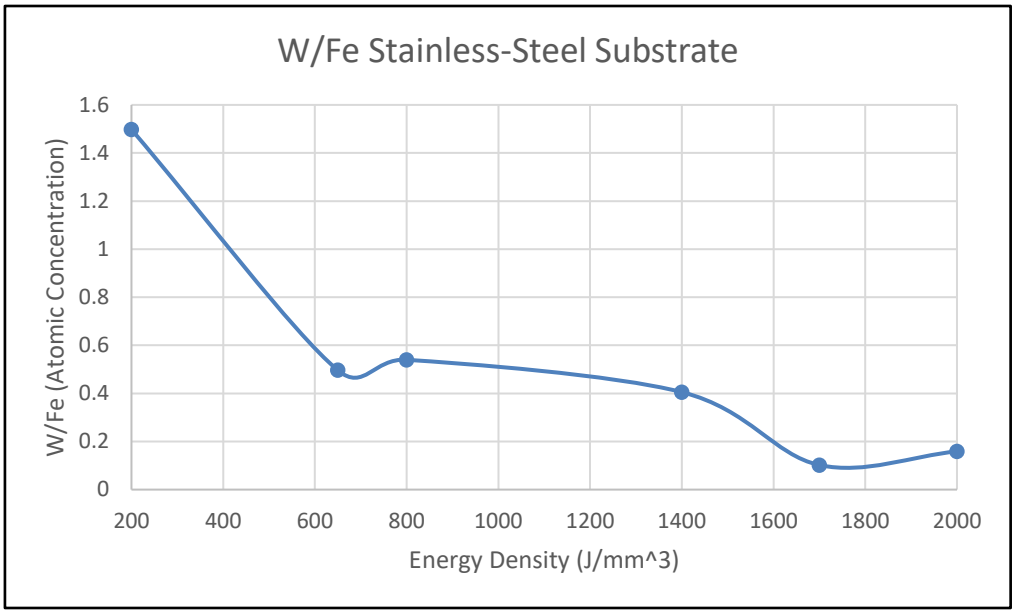

Figure 5-2-8: W/Fe Ratio of Stainless-Steel Substrate

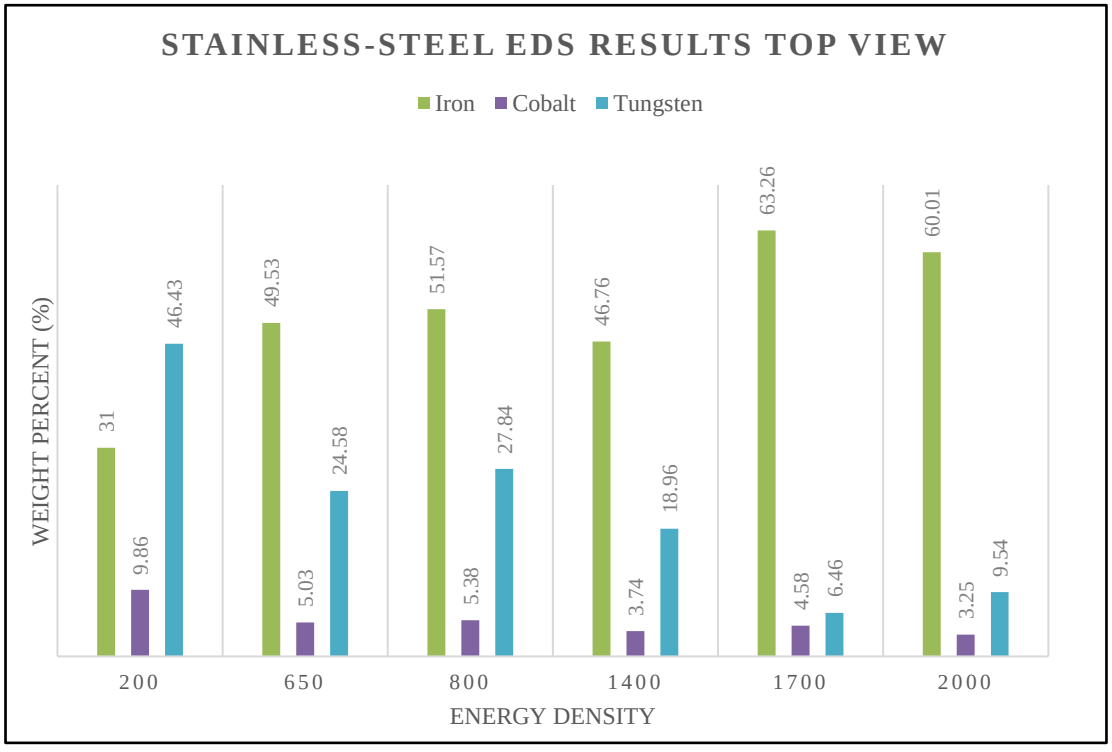

Figure 5-2-9: Element Weight Percent with Differing VED (Top View)

5.2.2. Cross Section of Stainless-Steel Substrate

The cross section of each printed specimen was done by use of wire EDM cutting. During the cutting the cut direction is perpendicular to the print direction and approximately located in the middle of each sample. Following the EDM cutting each specimen is polished using an alumina polishing powder with 0.005 micrometer particle size.

Observing the bar chart there are several observations that can be made. Percent weight of W in the lower energy density, 650 J/mm^3 or less, contain more than 50% weight of W. Following this energy density, the W drastically drops to a lower level that remains within a close range of 27-32.59% weight. Observing the energy density effects on the Fe weight percent located in the cross section are as follows. Fe in the energy densities from 650 J/mm^3 or less the percent weights range from 24.87-25.42% weight Fe. Energy densities greater than 650 J/mm^3 display a Fe weight percent greater than 50%. Both of these dramatic changes in percent weights of W and Fe located at the cross sections show that there is a significant effect on the material at energy density between 650-800 J/mm^3. Plotting the percent weight on the graph below provides several observations (Fig. 10). One is that unlike the W on the surface the cross-section percent weight does not follow as strong of a trend.

Observing the EDS images taken on the cross sections below displays what is occurring below the surface of the material (Fig. 5-11 to Fig. 5-16). Starting with the lowest energy density of 200 J/mm^3. The tungsten is very concentrated on the surface of the material, and the iron remains mostly below the tungsten layer. Having the iron concentrated below the printed surface explains why the lowest energy density produced the highest hardness. As the energy density increases in value one can observe that the iron continually increases its density into the surface of the coating causing the hardness value to decrease. Also, an important observation made from these images is that the tungsten is shown to be flowing deeper into the material as the energy density increases. A possible reason for this is that as the energy density increases is the Marangoni effect experienced below increasingly becomes prominent in the surface of the coating as the laser is in operation.

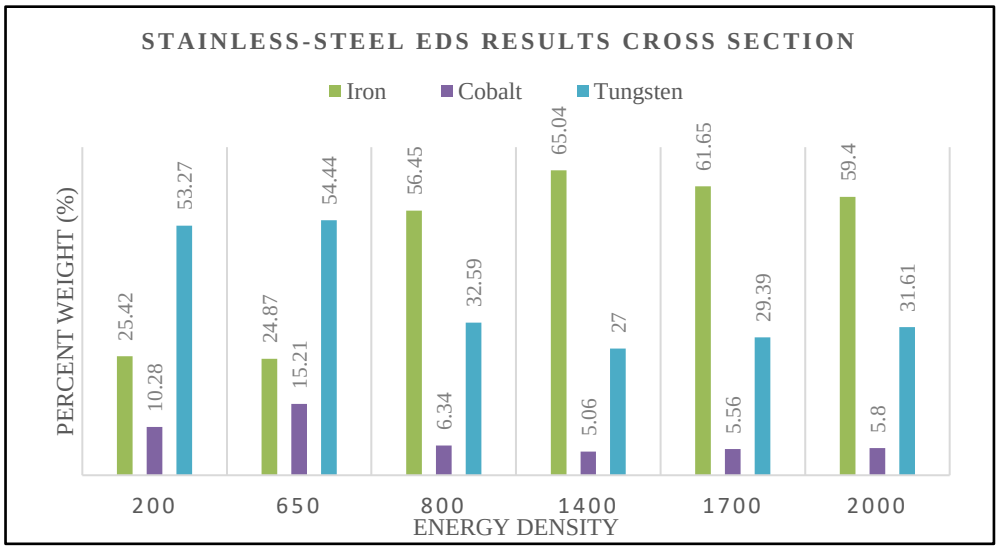

Figure 5-2-10: Element Weight with Differing Energy Densities (Cross

Figure 5-2-11: W and Fe Distribution within the Cross-Section (200 J/mm^3)

Figure 5-2-12: W and Fe Distribution within the Cross-Section (650 J/mm^3)

Figure 5-2-13: W and Fe Distribution within the Cross-Section (800 J/mm^3)

Figure 5-2-14: W and Fe Distribution within the Cross-Section (1400 J/mm^3)

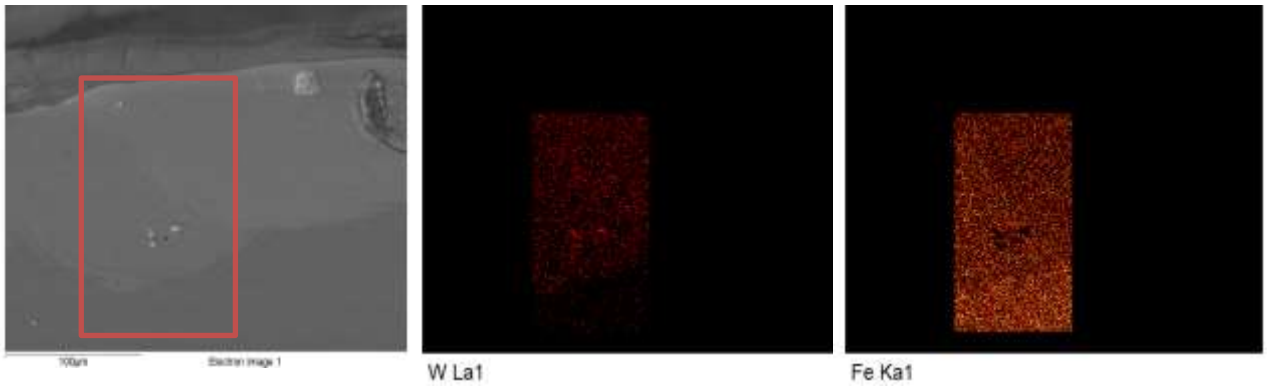

Figure 5-2-15: W and Fe Distribution within the Cross-Section (1550 J/mm^3)

Figure 5-2-16: W and Fe Distribution within the Cross-Section (2000 J/mm^3)

5.3. Hardness of Stainless-Steel Substrate

Observing the data displayed, the hardness value is represented by the upper line and the standard deviation is represented by the lower line (Fig. 17). Hardness values measured at the surface of the sample displays the highest hardness readings with low energy densities. The highest hardness observed was taken at 350 J/mm^3 equaling 1081.78 (HV), and the lowest value located at 1400 J/mm^3 equaling 663.18 (HV). Energy densities that follow 350 J/mm^3 display significant hardness loss. There also is a significant decline in hardness observed between the energy densities of 500-800. After which the values remain within a range of 663.18-761.2 (HV) with the exception of one outlier located at 1750 J/mm^3 equaling 923.44 (HV). Concluding that improving the surface hardness has the greatest effects using lower energy densities, and as the energy density increases the hardness decreases until a certain level after which the hardness value stays relatively linear.

This same trend observed in the averages of the hardness value is also found in the standard deviations of each sample as well. Showing that the standard deviation between the hardness readings is higher at the lower energy density, exceeding 200 (HV) between 200-650 J/mm^3, and experiences a significant decline after which the values become relatively linear. Falling between the values of 69.27-123.9 (HV) in standard deviation in the energy densities higher than 650 J/mm^3. One outlier located at 1700 J/mm^3 contains a standard deviation of 175.8 (HV). The conclusion that may be drawn from this data is that though the lower energy density does provide the higher hardness the low energy density also is highly inconsistent and ununiform. The higher energy

levels provide a lower range of values for the hardness. Meaning that prints consistency is higher with higher energy density.

Taking ten hardness values of the substrate, a stainless steel, the hardness value averaged 245 HV. Using the average hardness of the substrate, as a point of comparison to the increase in surface hardness observed from the surface exposed to the sintered WC-Co17 power. Figure seventeen displays the percentage increase in the surface hardness of the substrate after the printing has occurred. The highest increase in hardness is observed at 350 $\boldsymbol{J/mm^3}$ equaling 442% increase in the surface hardness. The lowest increase in surface hardness observed equaled 271% at 1400 J/mm^3. Even the minimum percentage increase poses a significant increase in the surface hardness showing that SLM of WC-Co17 exhibits high potential for the use of surface hardness, improvement on metallic surfaces.

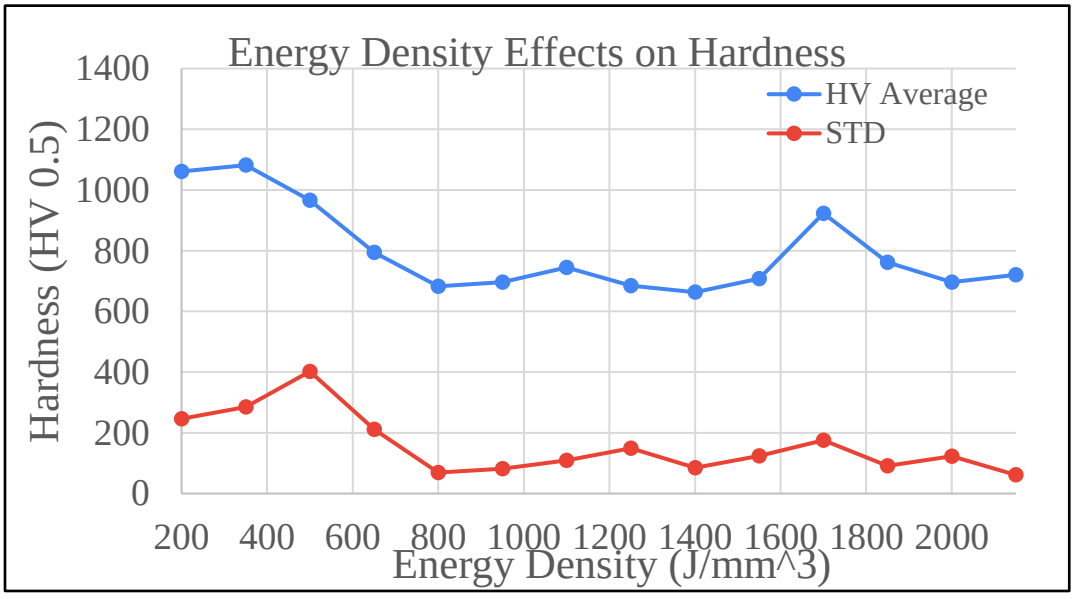

Figure 5-3-17: Hardness (HV) Results on Stainless-Steel Substrate

5.4. Summary

Summarizing the findings of this investigation, serveral conclusions are drawn that will influence the parameters selected for the H13.

Uniformity and coating characteristics varied as a function of energy density. Higher energy density resulted in the increase in track uniformity, decrease in size and quantity of cracks, and decrease in the number and size of spatter. The cause for these results is potentially due to the increased melt pool uniformity due to better melting at higher energies.

Tungsten and iron concentrations observed on the top and cross section vary as a function of energy density. As energy density is progressively increased the surface coating progressively decreased in surface concentration of W and Co and increased depth of W found within the substrate This is potentially due to the increased alloying effect and Marangoni effect.

Hardness values of the surface coating vary as a function of the energy density. Lower volumetric energy density results in higher Vickers hardness and higher standard deviations of hardness values. Reasoning can be due to the decrease of W concentration on the surface, and the coating quality.

With this approach we are able to achieve surface coatings with significantly higher hardness compared to the parent substrate material.

6. EFFECT OF INITIAL SURFACE CONDITION AND VOLUMETRIC ENERGY DENSITY IMPARTED ON LAYER MORPHOLOGY ON H13 SUBSTRATE (RQ2)

H13 is the second substrate chosen for this investigation. The reasons for choosing H13 are the following. One, is that H13 is one of the more common materials used in metal forming dies. Also, H13 is already a hard tool steel, and this investigation was performed to determine if it is feasible to greatly increase the surface hardness of a material. Pictured below is an example of what the coated surface looks like after the laser processing has been complete (Fig. 6-1 to Fig. 6-2). Each coated area measures 5mmX10mm. As explained in the previous design of experiments section, each of the energy densities applied to the H13 will be conducted twice. One time will be on a H13 substrate that has only been machined. While the second run will be on a H13 substrate that has been lapped post machining. Shown below are two images of the surfaces of these two different conditions (Fig. 6-1 to Fig. 6-4). Surface roughness of the machined samples average 1.42μm, and the lapped surface averages 1.23μm. However, the significant difference between these two surfaces is the surface of the machined sample has a wave like surface texture going parallel to the cutting direction, and the lapped surface is uniform across the area. Resulting in the standard deviation of the machined samples to be 0.64μm, and the lapped samples to be 0.07μm. This is investigated for two reasons, one is to investigate if substrate surface roughness influences the coating quality, and second is to potentially cut down on cost and machine time for the process to be applied in real world application.

6.1. Optical Images of H13 Substrate

Optical imaging of the two H13 substrate conditions are analyzed under three different fields of view. Each coating is analyzed at 5X, 10X, and 20X under a bright field setting. Optical images for these samples are important for two main reasons. The first is to observe if there are any surface cracks that occurred during the laser processing. Secondly, optical images show there are any spatter on the surface of the

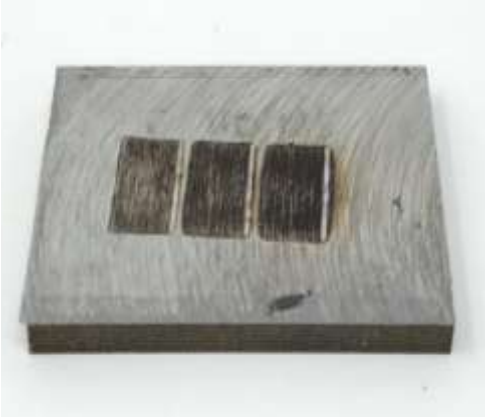

Figure 6-1-1: H13 Machined Substrate (950, 1100, 1250 J/mm^3) (5mm$x$10mm)

Figure 6-1-2: H13 Lapped Substrate (950, 1100, 1250 J/mm^3)

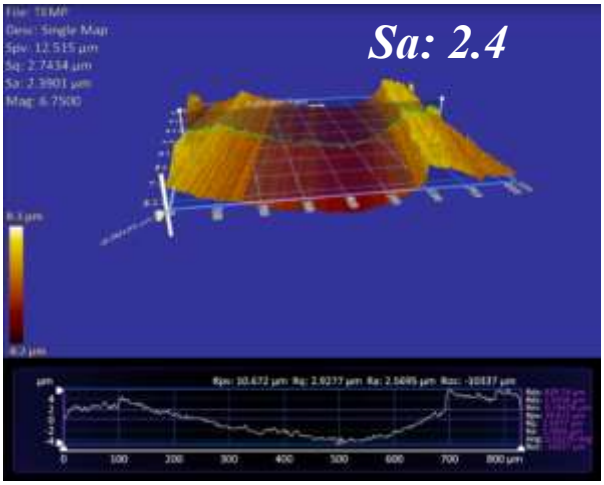

Figure 6-1-3: H13 Substrate Machined Surface

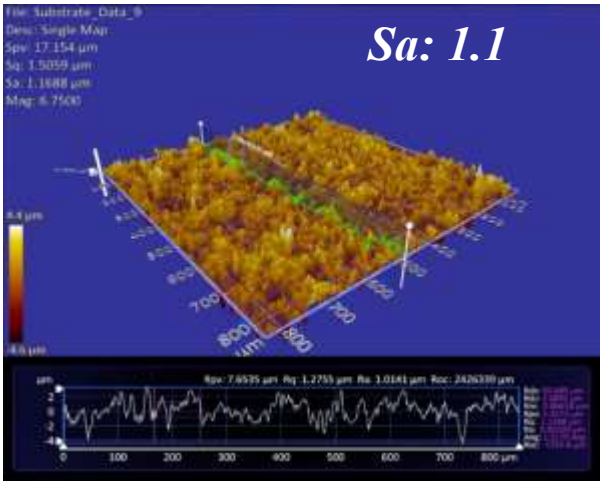

Figure 6-1-4: H13 Substrate Lapped

coated region. Observing these defects will allow the investigation to conclude which energy densities produce the best visual quality coating.

6.1.1. Optical Images of Lapped Surface

Observing the optical images below, (Fig. 4-8), similar trends are observed in the H13 substrate samples as seen in the stainless-steel samples. As energy density increase the amount of cracking and splatter seen on the surface of the coating decreases. However, cracking does continue to appear in the higher energy densities unlike the stainless-steel samples where cracking nearly is eliminated. One potential reason behind this continued observation of cracking can come from the substrate's thermal properties. Specifically, thermal conductivity of H13 equals 28.6 W/mK, and stainless steels between 304-316 range from 13-17 W/mK [10]. Having a significantly higher thermal conductivity, H13 will allow the heat produced by the laser to diffuse through the substrate at a much higher rate than that of the stainless-steel. This may cause thermally induced cracks by rapid change in temperature to easily propagate through the brittle carbide coating.

Spatter continues to greatly reduce its size and quantity as the energy density continues to increase. Spatter on the H13 substrate shows there may not be sufficient amount of energy applied to the powder. Reducing the bonding of the WC-Co17 powder to the surface of the H13 substrate before being dislodged from the surface and forming a splatter point. Spatter causes the surface of the coating to not be uniform across its area. Causing undesired surface finishes on the metal formed product. Minimizing the

cracking and splatter with the higher energy density applied to the powder will produce an increased homogenized surface on the lapped surface of a H13 substrate.

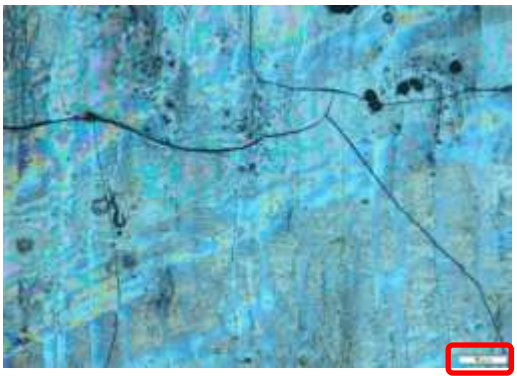

Figure 6-1-5: H13 Substrate Coating (500 J/mm^3) (All scale bars = 50 μm)

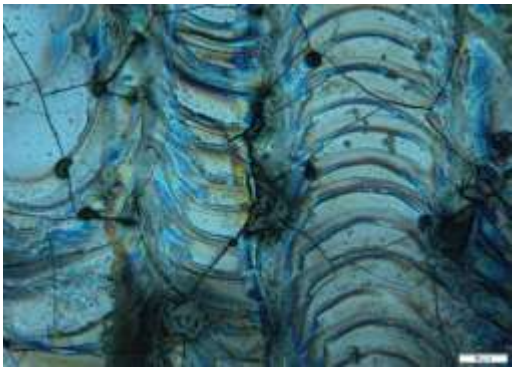

Figure 6-1-6: H13 Substrate Coating (800 J/mm^3)

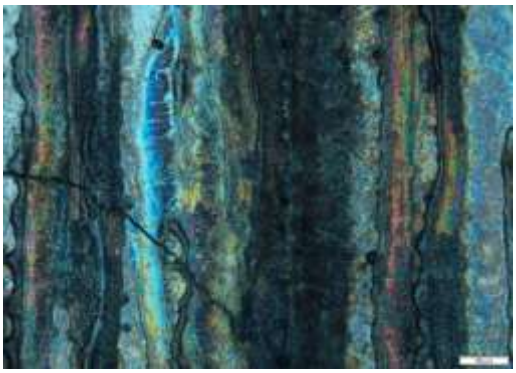

Figure 6-1-7: H13 Substrate Coating (1100 J/mm^3)

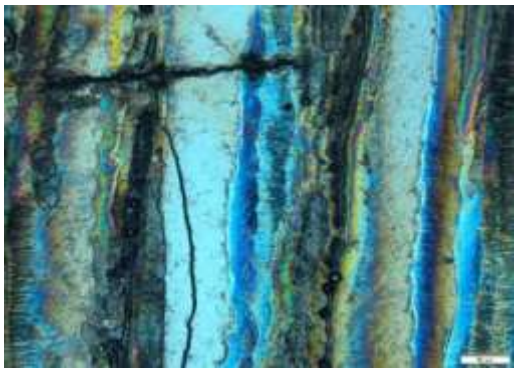

Figure 6-1-8: H13 Substrate Coating (1400 J/mm^3)

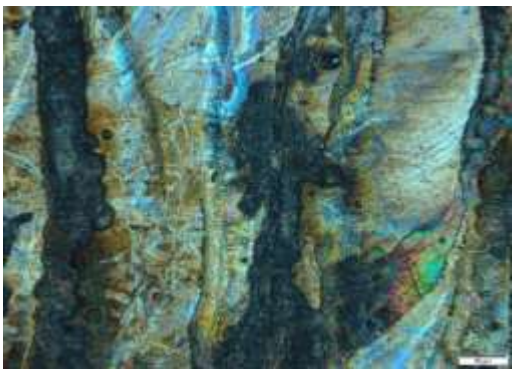

Figure 6-1-9: H13 Substrate Coating (1550 J/mm^3)

6.1.2. Optical Images of Machined Surface

Observing the optical images below, (Fig. 9-13), similar trends are observed in the H13 substrate samples that are machines compared to the previously lapped surfaces of H13 substrate samples. As energy density applied to the powder increases the amount of cracking and splatter on the surface of the coating decreases. Cracking does again continue to appear in the higher energy densities with significant reduction in frequency and size. Splatter, like the previous H13 substrate, decreases in size and quantity. Comparing the optical images between the lapped and machined surface finished substrates there is no distinguishable difference between the two. Both the machined and previously discussed lapped substrates show the same trend in higher energy densities reduce the cracking and splatter on the top surface of the coating. The top surface of the samples when examining the print tracks both improve in uniformity as well with the increased energy density.

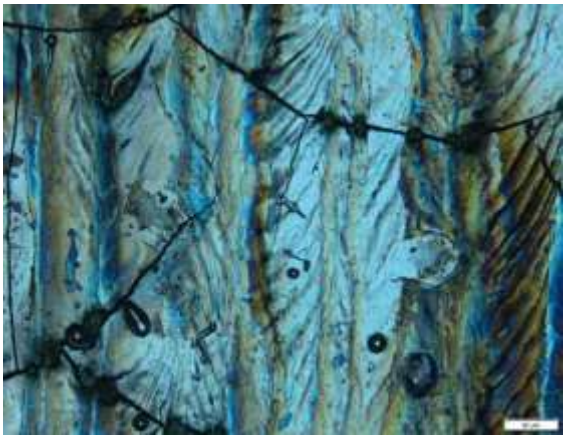

Figure 6-1-10: H13 Substrate Coating (500 J/mm^3) (All scale bars = 50 μm)

Figure 6-1-11: H13 Substrate Coating (800 J/mm^3)

Figure 6-1-12: H13 Substrate Coating (1100 J/mm^3)

Figure 6-1-13: H13 Substrate Coating (1400 J/mm^3)

Figure 6-1-14: H13 Substrate Coating (1550 J/mm^3)

6.2. Surface Roughness of H13

Surface roughness profiles of the coatings are taken post laser processing on both the lapped and machined surfaces. As shown in the previous figures, there is no significant difference in average surface roughness (Fig. 12-13). The major difference comes from the standard deviations between the lapped and machined surfaces. Post coating, the surfaces are reexamined for influences in the increasing energy densities, and the influence of the starting surface roughness of the substrate.

6.2.1. Lapped H13 Substrate

Observing the H13 samples with a lapped surface, there is a significant difference in surface roughness as energy density increases. As seen in the preliminary investigation with stainless-steel as the substrate is exposed to higher energy densities the surface roughness decreases. Shown in the figures below, two of the surface profiles taken, one profile is taken on the sample with the energy density of 500 J/mm^3 and the second at an energy density of 1550 J/mm^3 (Fig. 6-14 – Fig.6-15). Between these two

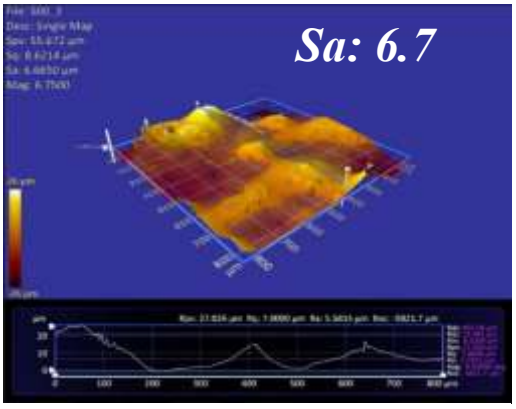

Figure 6-2-15: Lapped H13 Surface Roughness (500 J/mm^3)

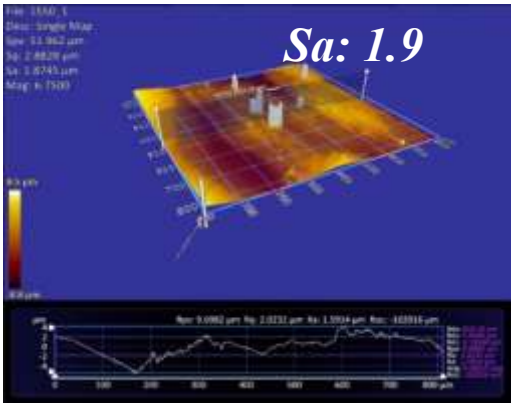

Figure 6-2-16: Lapped H13 Surface Roughness (1550 J/mm^3)

profiles there is more than a 350% decrease in the roughness when using the energy density of 1550 J/mm^3 to 500 J/mm^3. Taking these profiles of each energy density tested, a graph is created to show the trend of the surface roughness and the corresponding standard deviations (Figure 6-18). Observing the data points for the lapped surface, there is a continuous trend in decreasing the surface roughness while increasing the energy density. The standard deviations of the surface roughness values measured at each energy density remain below 1 micrometer with exception to the energy density of 650 J/mm^3.

6.2.2. Machined H13 Substrate

Observing the H13 samples with the machined surface, similar to the lapped surface, there is a significant difference in surface roughness as the energy density increases. Shown in the figures below, two surface profiles are displayed, one profile is taken at the energy density of 500 J/mm^3 and the second at an energy density of 1550 J/mm^3 (Fig. 17-18). Between these two profiles there is more than a 280% decrease in the surface roughness when using the energy density of 1550 J/mm^3 instead of 500 J/mm^3. Taking these profiles of each energy density, the graph created to show the trend of the surface roughness and the corresponding standard deviations are plotted for the machined substrate samples (Figure 6-19). Observing the data points for the machined surface samples, there is again is a continuous trend in decreasing the surface roughness while increasing the energy density. The standard deviations of the surface roughness values measured at each energy density remain below 1 micrometer.

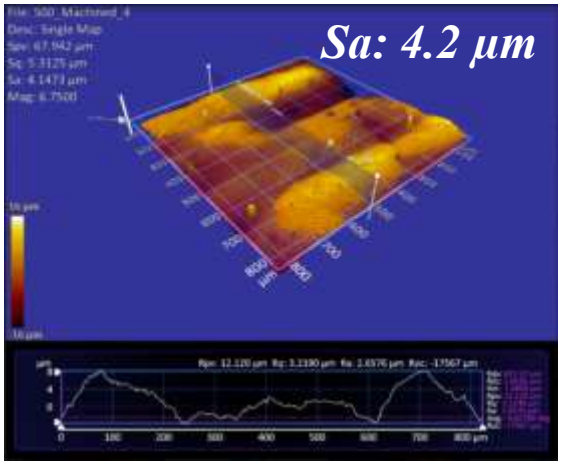

Figure 6-2-17: Machined H13 Surface Roughness (500 J/mm^3)

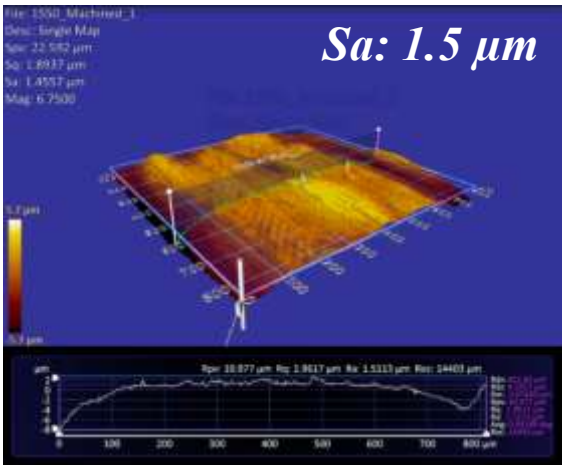

Figure 6-2-18: Machined H13 Surface Roughness (1550 J/mm^3)

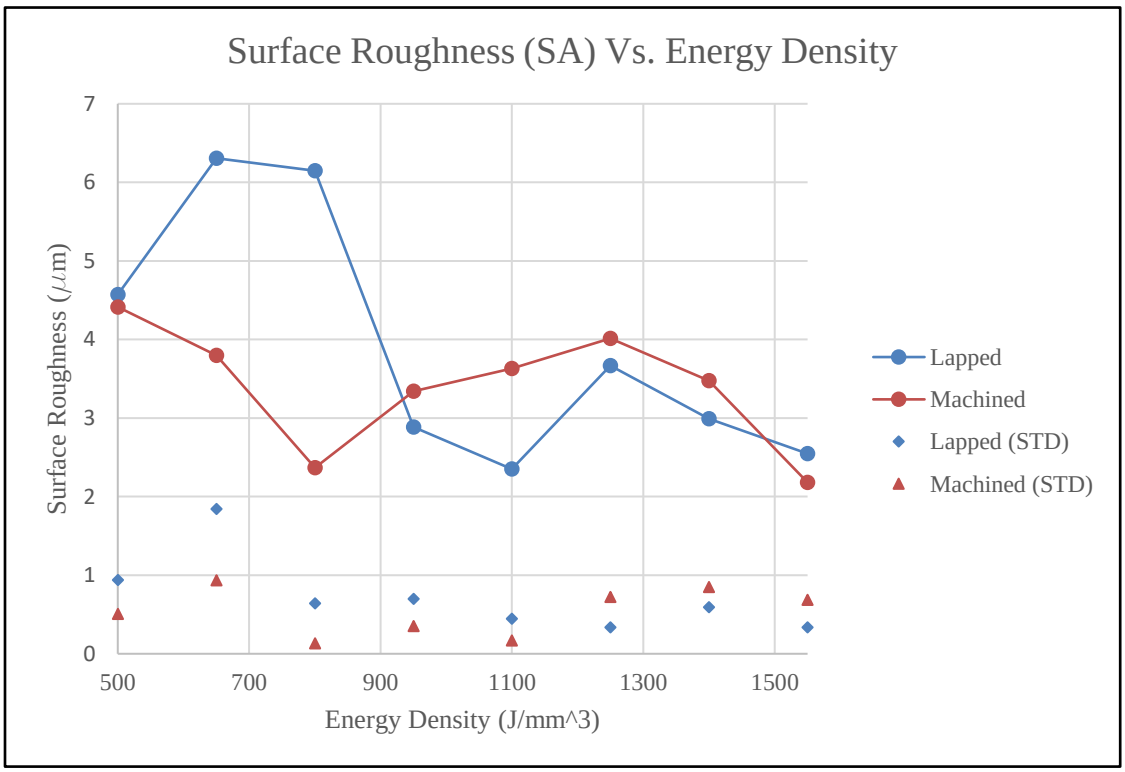

Figure 6-2-19: Surface Roughness and STD for Lapped and Machined Surface Finishes

Comparing both the lapped and machined H13 substrate surface roughness values there are several observations to be made. The first observation is that in both cases as the energy density increases the surface roughness decreases as well. Beyond the energy density of 950 J/mm^3 both sample types surface roughness still decreases but with less effect in decreasing the roughness average. Differences between the lapped and machined samples coated surface roughness are the following. One, the standard deviation of values for the lapped substate appear to have a downward trend. While the machined substrate seems to remain within a bound of 0.133-0.933 micrometers with no obvious trend. In conclusion, substrate surface finish does not appear to influence the resulting surface roughness of the coating applied onto the substrate.

6.3. Top Surface Elemental Composition of H13 Substrates Coated Area

Analysis of the elemental composition of the surface of the coating enables this investigation to identify causes in the trends seen in the above analysis. Energy-dispersive X-ray spectroscopy is performed on each of the energy densities used on the H13 substrates. Observing the SEM images and combine mapping images below of the low energy density 500 J/mm^3 (Fig. 6-20 through Fig. 6-21). Both the lapped and machined surfaces of the H13 substrate exhibit similar elemental concentrations on the surface of the coating at this energy density. In both instances the lighter regions of the coating appear to contain a higher concentration of tungsten. While the darker regions contain higher concentrations of the iron. Observing no significant difference between the two H13 substrates exposed to the energy density of 500 J/mm^3 supports the evidence that at low temperatures both coatings exhibit similar hardness's. Further

support to these observations is seen in table 6-1 and table 6-2, where the atomic concentrations of the elements within the combined map region is quantified. Atomic concentration of tungsten located on the top surface of the coatings has approximately three percent difference between the two different substrates.

Figure 6-3-20: Lapped H13 SEM Image (500 J/mm^3)

Figure 6-3-21: Lapped H13 Combined Map Image (500 J/mm^3)

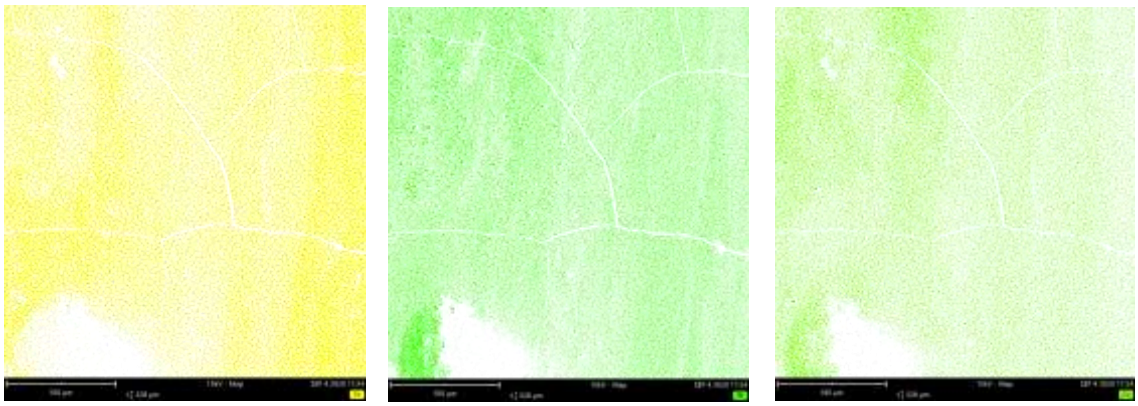

Figure 6-3-22: Lapped H13 SEM Image (500 J/mm^3) (Iron, Tungsten, Cobalt)

Table 6-3-1: Lapped H13 Atomic Concentration (500 J/mm^3)

Element Symbol	Element Name	Atomic Conc.	Weight Conc.
W	Tungsten	23.3	64.2
C	Carbon	23.2	4.1
O	Oxygen	22.3	5.3
Fe	Iron	20.1	16.7
Co	Cobalt	9.6	8.5
Cr	Chromium	1.2	0.9

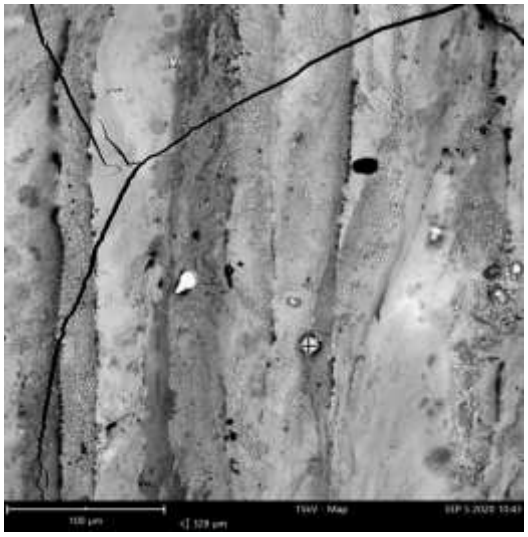

Figure 6-3-23: Machined H13 SEM Image (500 J/mm^3)

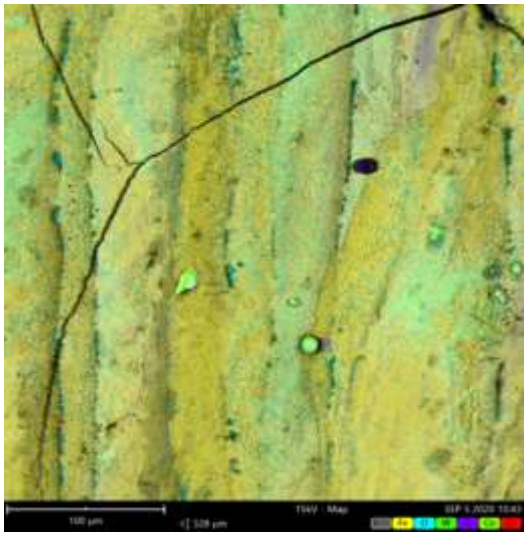

Figure 6-3-24: Machined H13 Combined Map Image (500 J/mm^3)

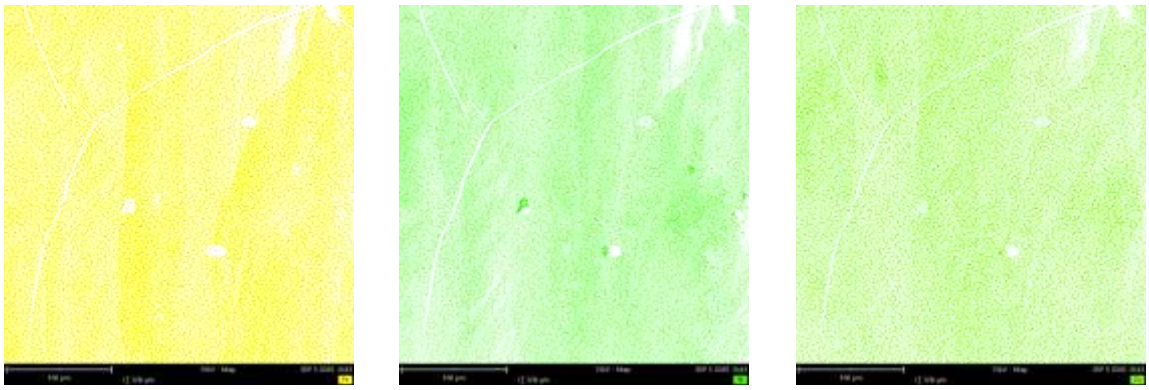

Figure 6-3-25: Machined H13 SEM Image (500 J/mm^3) (Iron, Tungsten, Cobalt)

Table 6-3-2: Machined H13 Atomic Concentration (500 J/mm^3)

Element Symbol	Element Name	Atomic Conc.	Weight Conc.
Fe	Iron	30.1	23.4
O	Oxygen	26.5	5.9
W	Tungsten	24.0	61.7
C	Carbon	10.3	1.7
Co	Cobalt	6.5	5.3
Cr	Chromium	2.4	1.7

Following the energy density of 500 J/mm^3, the lowest energy density, observation of the highest energy density, 1550 J/mm^3, is observed (Fig.6-8 through Fig. 6-10). Observing the lapped sample, similar to what was seen in the stainless-steel samples, there is a significant decrease in the atomic concentration of tungsten. The combined mapping image shows a concentration of tungsten located at the edge of the track lines, and a concentration of iron spread throughout the mapped area. Having the significant loss of tungsten, 51.41% decrease, on the surface of the coating supports the cause of decreasing hardness in the coating as the energy density increases (Table 6-3). One potential leading cause to this is the Marangoni effect, where the substrate material is circulated to the surface of the melt pool and the coating material is embedded into the subsurface of the substrate. Atomic concentration of the tungsten on the H13 substrate that was only machined and the energy density of 1550 J/mm^3 is applied yielded significantly different results. Tungsten still decreased in the atomic concentration. However, the decrease percentage was 18.85%, making the concentration of tungsten 2.73 times higher on the machined surface versus the lapped surface. This supports the results of the hardness testing conducted above. Where the surface hardness of the coating remains above 1000 HV, even when using a higher energy density. The percentage difference in tungsten concentration on the top surface between the lapped and machined H13 samples exposed to 1550 J/mm^3 is 53%. Having a difference of more than 50% tungsten concentration on the surface explains the reasoning behind the difference in the hardness readings taken at the higher energy densities.

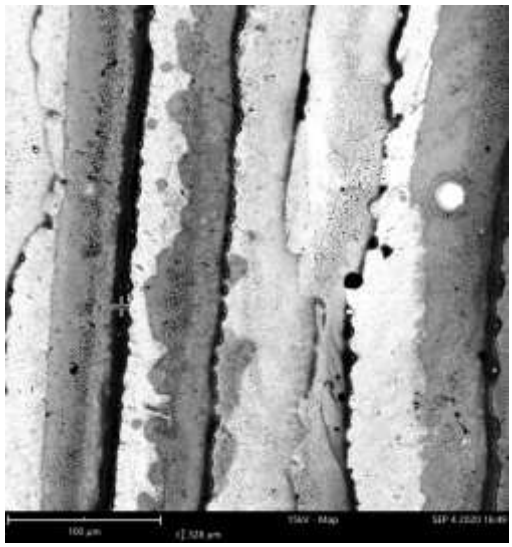

Figure 6-3-26: Lapped H13 SEM Image (1550 J/mm^3)

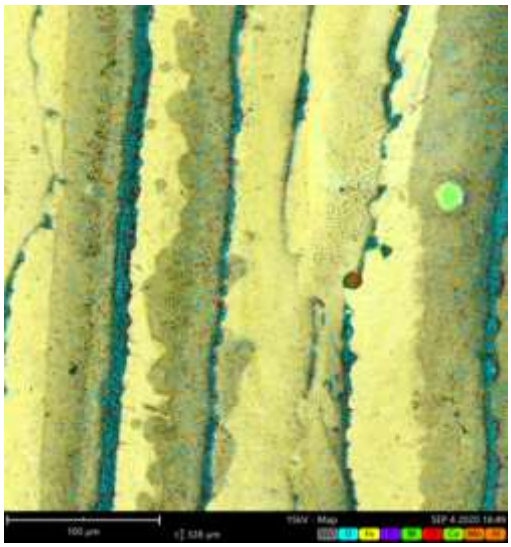

Figure 6-3-27: Lapped H13 Combined Map Image (1550 J/mm^3)

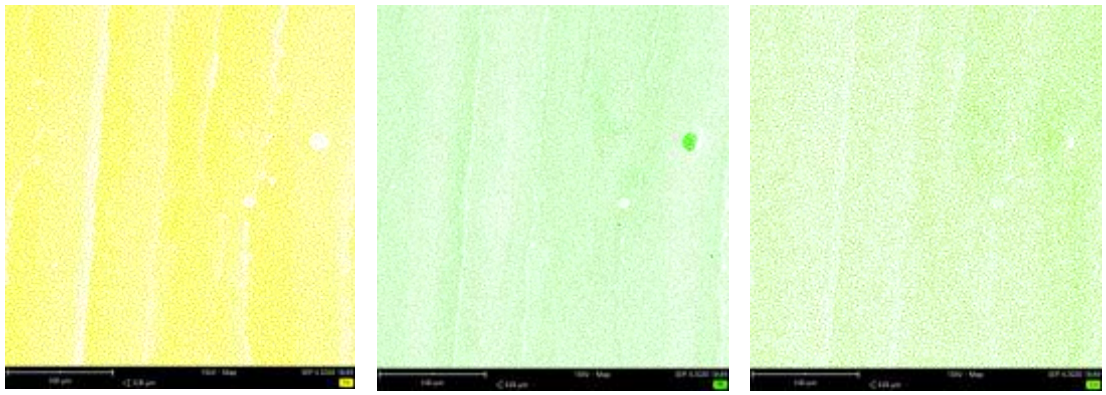

Figure 6-3-28: Lapped H13 SEM Image (1550 J/mm^3) (Iron, Tungsten, Cobalt)

Table 6-3-3: Lapped H13 Atomic Concentration (1550 J/mm^3)

Element Symbol	Element Name	Atomic Conc.	Weight Conc.
O	Oxygen	38.55	12.66
Fe	Iron	28.95	33.19
C	Carbon	13.94	3.44
W	Tungsten	11.36	42.88
Cr	Chromium	3.14	3.36
Co	Cobalt	2.58	3.12

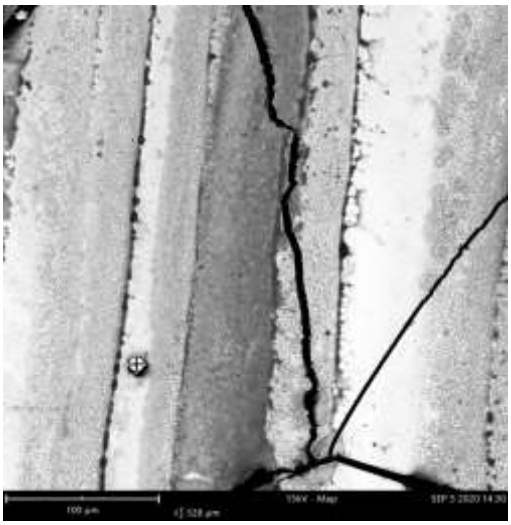

Figure 6-3-29: Machined H13 SEM Image (1550 J/mm^3)

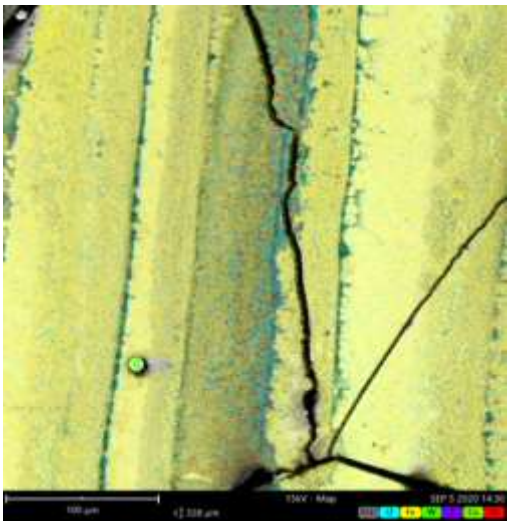

Figure 6-3-30: Machined H13 Combined Map Image (1550 J/mm^3)

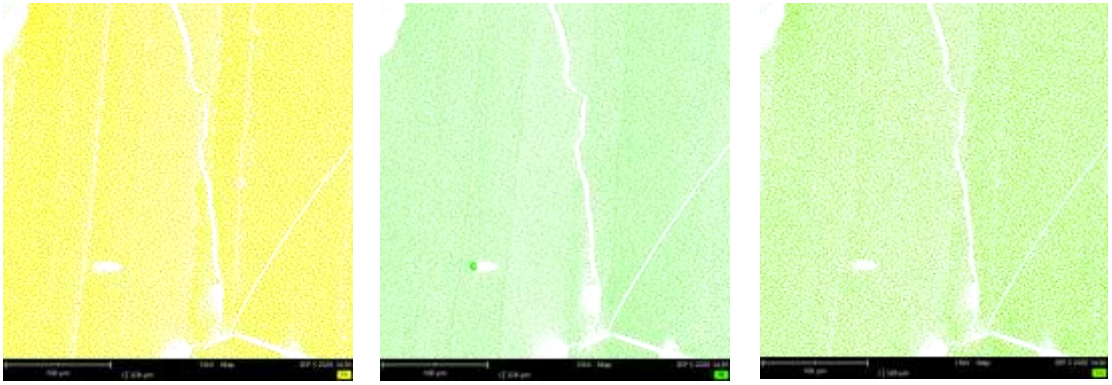

Figure 6-3-31: Machined H13 SEM Image (1550 J/mm^3) (Iron, Tungsten, Cobalt)

Table 6-3-4: Machined H13 Atomic Concentration (1550 J/mm^3)

Element Symbol	Element Name	Atomic Conc.	Weight Conc.
O	Oxygen	32.37	8.13
Fe	Iron	30.59	26.80
W	Tungsten	19.55	56.38
C	Carbon	9.75	1.84
Co	Cobalt	4.98	4.60
Cr	Chromium	2.77	2.26

Potting the elemental compositions on bar charts, the difference in surface elemental composition between a lapped and machines surface of H13 is observed. Observing results taken on the lapped H13 substrate, there is a decline similar to that seen in the stainless-steel (Fig. 6-33). At low energy densities the tungsten concentration on the surface of the coating is the highest values, and as the energy continues to increase the tungsten concentration declines. Cobalt follows this similar trend. A noticeable shift at the point of decline in tungsten concentration occurs when using the H13 as the substrate. Previously, the significant decline occurred at energy densities beyond 650 J/mm^3. On H13, the decline does not occur until the energy densities beyond 800 J/mm^3. Reasons for the shift to a higher energy density before significant reduction in tungsten concentration are due to the H13 material characteristics. H13 exhibits higher heat resistance then that of stainless-steels. Being more resistant to heat will inhibit the melt pool to experience the Marangoni effect.

Observing the H13 substrate with the machined surface finish, a different trend occurs compared to the lapped surface finish (Graph 6-2). As expected, the tungsten concentration on the surface of the coating when using the lower energy density is within the same range as seen in the lapped sample. However, as energy density increases the tungsten does not experience a dramatic drop in concentration as seen in the lapped samples. Instead the concentration of tungsten experiences a slight decline in tungsten concentration, and decreases closely to a linear decline. Observing this trend in this part of the investigation supports the data stated previously, where the hardness of the machined coating remains significantly harder than the coating of the lapped sample

at the higher energy densities. Cobalt concentration remains within a range of concentrations of 3.1-6.6 percent concentration, and has no obvious trend occurring as the energy density is increased.

The final graph to analyze from the elemental concentrations on the surface of the H13 substrates is a tungsten to iron percent concentration ratio (Figure 6-31). Analysis of the two plotted lines, one for the lapped and the other for the machined surface finish, there clearly is a difference in the ration of tungsten to iron concentration between the two different surface finishes. For the lapped surface finish samples, the tungsten to iron concentration ratio drops greatly beyond the energy density of 800 J/mm^3. Having a ratio of tungsten to iron less than 0.4 for the energy densities higher than 800 J/mm^3. Compared to the machined surfaces of the H13 substrate, the ratio of tungsten to iron concentration remains above 0.5, and for all cases except for two the ratio is above 0.6. Taking the two lowest concentration ratios from the different substrate surface finishes, at minimum there is a 23.1% decrease in tungsten to iron concentration ratio from machined to lapped surfaces. This too supports the reasoning of the machined samples having a higher hardness value compared to that of lapped.

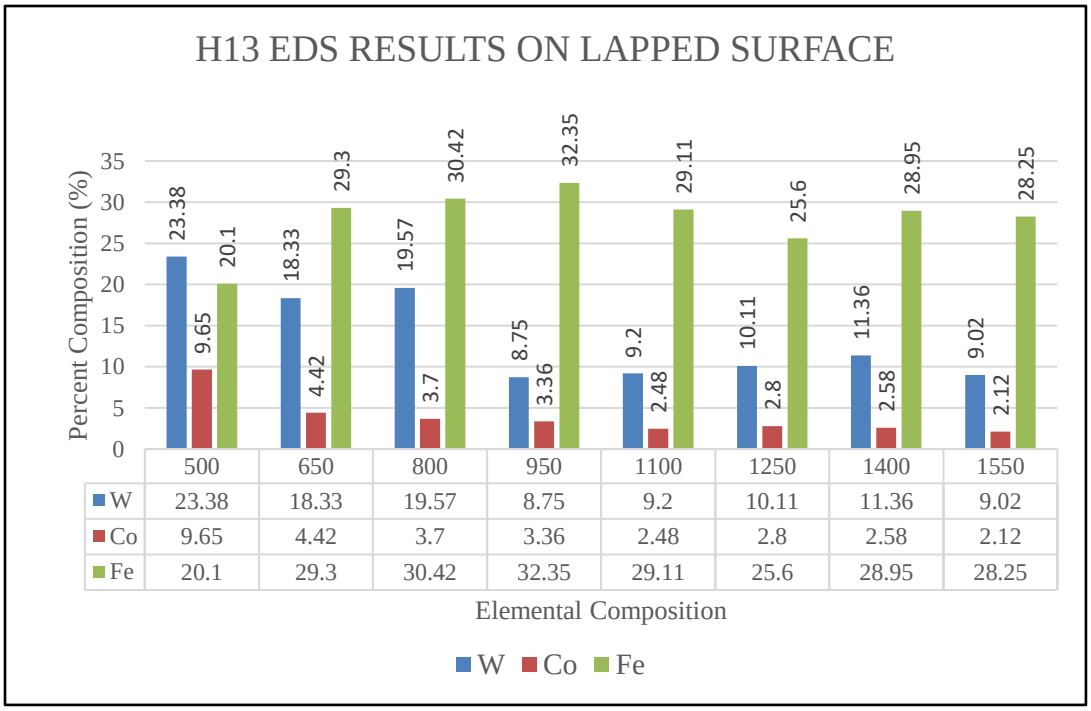

Figure 6-3-32: Lapped H13 Tungsten, Cobalt, and Iron Elemental Compositions

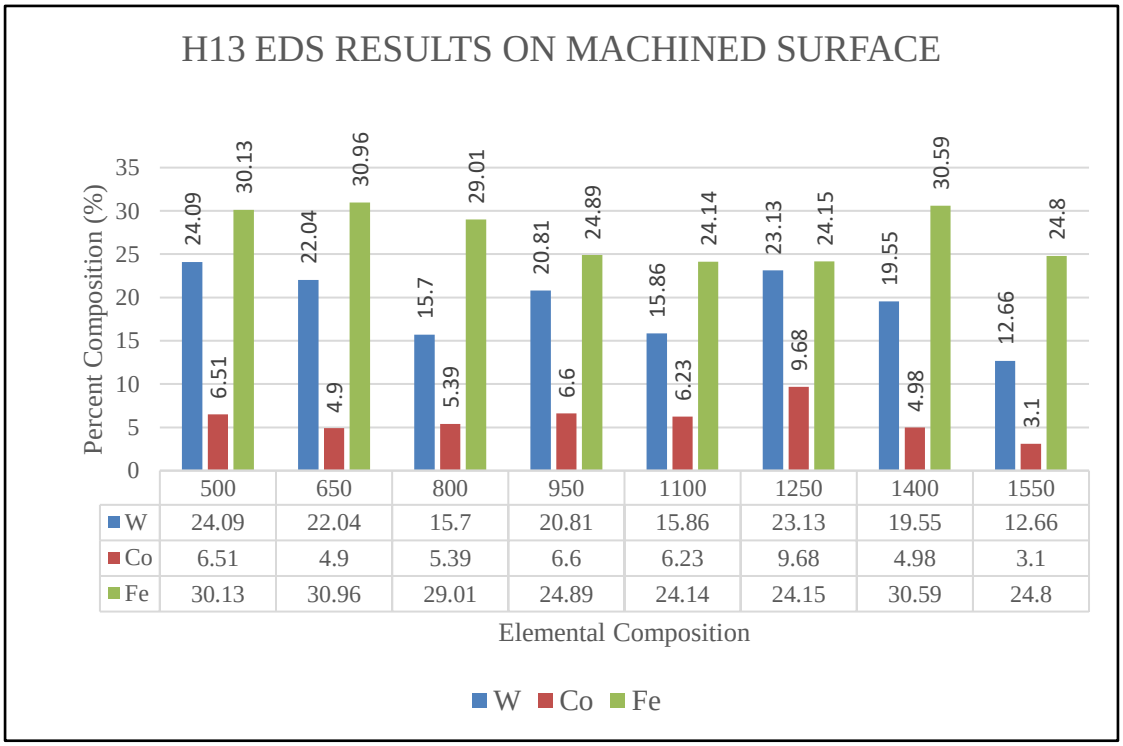

Figure 6-3-33: Machined H13 Tungsten, Cobalt, and Iron Elemental Compositions

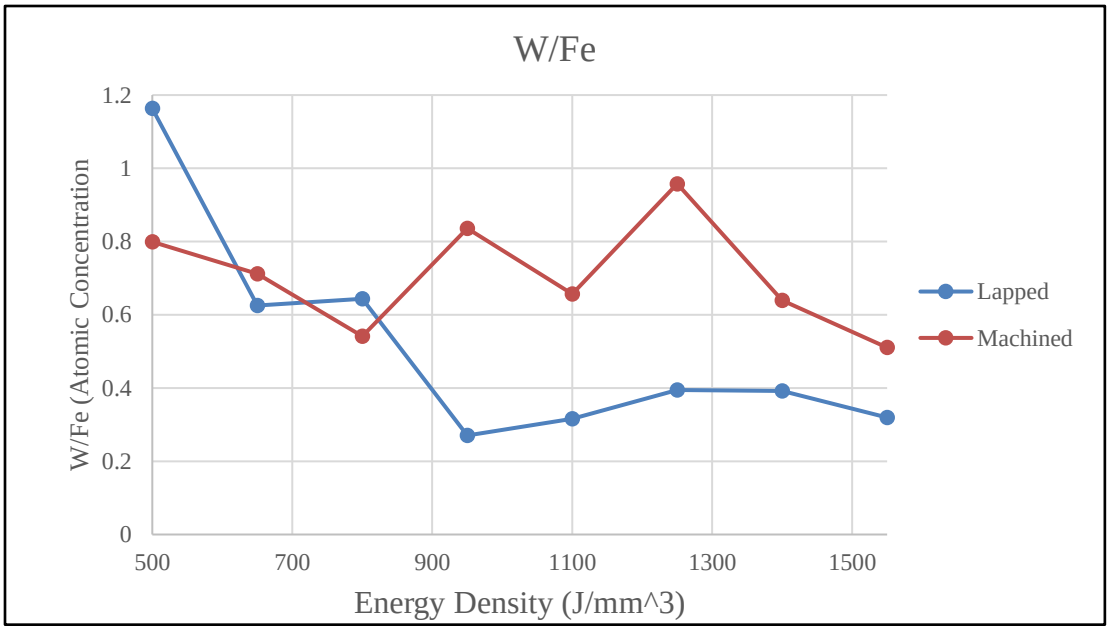

Figure 6-3-34: Tungsten/Iron Elemental Ratio

6.4. Summary

Both lapped and machined surfaces print quality and uniformity varied as a function of energy density. Higher energy density imparted onto the powder layer decrease size and quantity of cracks and decrease number and size of spatter. Surface roughness of the coating varied as a function of energy density for lapped and machined surfaces with the same observed trend. Higher energy density imparted lead to lower surface roughness and standard deviation.

Lapped samples show tungsten concentrations observed on the top surface vary as a function of energy density. Higher energy density results in lower concentration of W observed on the surface of the coating. Coating hardness varied as a function of energy density as well. Lower energy density results in higher Vickers hardness

and standard deviation. Possible reasons for the lapped sample to yield such results include higher uniformity of the melt pool, increased alloying, and increased Marangoni effect.

Machined samples yield results different from that of the lapped samples. Tungsten concentrations observed on the top surface remain within a bound regardless of energy density. As higher energy densities are utalized the W is retained with higher concentration compared to that of lapped. Coating Vickers hardness values remain high independent of energy density. Higher energy densities retain hardness values above 1000 HV. Possible reasons for the machined sample to yield such different results could be the difference in the parent substrate surfaces when examining the surface on the frequency spectrum. Machined surfaces have larger peak to vally highs, and larger periods when compared to the lapped surfaces. This can influence the powder during processing and aid in the retension of powder inside of the meltpool. Also, increased uniformity of the melt pool could be a possible reason behind these results.

7. CONCLUSIONS AND FUTURE INVESTIGATION

7.1. Conclusions

In conclusion to this investigation we successfully fabricated hard carbide coatings on the stainless steel and H13 substrates. Correlations in energy density based process parameters with surface morphology and properties are drawn at the conclusion of this investigation. As higher energy density in imparted on the surface of the powder layer this leads to a general reduction in cracking and spatter on the coating across both substrates, and percentage of W reduced as percentage of iron increased as energy density increases in general. The one exception being the machined surface of the H13 substrate. Reasoning for the reduction in the W composition can be an increasing alloying phenomenon occuring at the surface. This process results in a much harder surface compared to that of the parent materials original surface hardness. Stainless-Steel exhibited a trend that as the energy density is increased, surface hardness decreases. H13 Substrate material yeilds two different results. As the energy density is increased, surface hardness decreases for Lapped H13, and for the machined surface of H13 the hardness value remains relatively constant when increasing the energy density. After performing the same laser-based process on the lapped H13 substrate a similar trend is observed compared to that of the stainless steel. With the major difference being that the significant drop in hardness shifted to a higher energy density (950 J/mm^3). As opposed to stainless steel having a significant drop in hardness observed at (650 J/mm^3). Discovery of the influence of the surface finish's effect of hardness extends the

possibility to further improve the coating characteristics after a single laser processing scan such as surface roughness without compromising the hardness significantly.

Possible reasoning behind the reduction in surface hardness, surface roughness, elemental composition, and spatter and cracking comes from the melt pool formed during the laser processing. Using lower energy density results in high scan speeds. High scan speeds can cause melt pool instability resulting in melt splashing, or little liquid content in melt pools causing the formation of spatter on the surface of the layer coating [11]. Having less material located at the point of the laser beam, due to spatter, also causes greater amounts of thermal stress in the coating. Experiencing higher thermal shock, leads to the significant cracking. As the energy density is increase in the experiments the melt pool is able to become increasingly stabilized. Resulting in the reduction of the spatter and cracking seen on the coating surface. Plateau-Rayleigh instability also influences the spatter and crack formation observed in the samples [11]. Allowing the material sufficient time to form a stabilized melt pool reduces the spatter and crack formation due to recoil pressure, insufficient energy density, thermal shock and stress, and liquid inside the melt. Substrate surface characteristics, prior to processing, influence the resulting coating characteristics in several ways. As noted above, the major difference between the lapped and machined surface is not the actual surface roughness average, but instead the value from the trough to peak (Fig. 6-2 and Fig. 6-3). When the laser scans over the lapped surface the powder is free to move in any direction causing spatter and powder loss. Recoil pressure produced by the laser during the processing is unrestricted as well causing more powder material loss. To reduce the

effects of powder removal and improved melt pool stability higher energy densities are used. The removal of powder at higher energy densities is reduced. However, for the lapped substrate surfaces, the Marangoni effect increasingly allows substrate material to be melted and flow to the surface of the coating. This explains the reasoning in the hardness values decreasing with increasing energy density on the substrates with lapped surfaces. When the laser scans over the powder with a machined surface the powder has limited movement capabilities because of the peak to trough distance. On the machined surface the powder is able to settle between the two peaks from the machining tool, and once settled the powder now has resistance from moving out of the area due to the peaks providing some resistance to movement. As the laser process begins an increased amount of powder is able to be retained inside the melt pool without dislodging. During high energy density processing, having the increased powder material reduces the Marangoni effect of substrate material flow to the surface of the substrate. The increased energy density is utilized to stabilize the melt pool, and increasing the amount of tungsten carbide-cobalt 17 powder residing in the melt pool reduces the amount of substrate material melted and circulated to the surface of the coating. Observing the EDS results above of the machined surface supports this conclusion to reducing the Marangoni effect on the substrate material.

7.2. Future Investigations

Further research to be conducted on this investigation is to determine at what energy density if any does the hardness of a machined surface dramatically drop on a

H13 substrate. Also, surface defects and roughness can be further improved by applying the higher energy densities through the reduction of melt pool instability. If the decrease in hardness remains linear then predictions can be made as to what the elemental composition and hardness will be when using a certain energy density. Further investigation in the effects of original surface profiles of substrates also can be conducted to better optimize the print quality. Use of a high-speed thermal imaging camera may also be beneficial for observing the melt pool formation and print track formation through the laser processing. This will identify the substrates surface characteristics influence on the melt pool. Perform XRD on the surfaces for phase identification within the coating to better understand the morphology after coating the material. Quantify the residual stress states against process parameters so that delamination can be minimized, and to determine the strength of the coating. Tribological testing of the surfaces too can be investigated to determine the surface friction and lubrication intrapment.

8. REFERENCES

[1] D. Zhou, C. Du, J. Siekirk, J. McGuire, X. Chen, and B. S. Levy, “A practical failure limit for sheared edge stretching of automotive body panels,” *SAE Tech. Pap.*, no. April 2010, 2010, doi: 10.4271/2010-01-0986.

[2] Jiang, Wenping, and Pal Molian, “Nanocrystalline TiC powder alloying and glazing of H13 steelusing a CO laser for improved life of die-casting dies.” *Surface and Coatings Technology*, vol. 135, no. 2-3, 2001, pp. 139–149, doi:10.1016/s0257-8972(00)01075-6.

[3] H. C. Kim, I. J. Shon, J. E. Garay, and Z. A. Munir, “Consolidation and properties of binderless sub-micron tungsten carbide by field-activated sintering,” *Int. J. Refract. Met. Hard Mater.*, vol. 22, no. 6, pp. 257–264, 2004, doi: 10.1016/j.ijrmhm.2004.08.003.

[4] S. Montgomery, D. Kennedy, and N. O. Dowd, “PVD and CVD Coatings for the Metal Forming Industry,” pp. 1–13, 2010.

[5] R. S. Khmyrov, V. A. Safronov, and A. V Gusarov, “Obtaining Crack-free WC-Co Alloys by Selective Laser Melting,” *Phys. Procedia*, vol. 83, pp. 874–881, 2016, doi: 10.1016/j.phpro.2016.08.091.

[6] C. Tan, K. Zhou, W. Ma, B. Attard, P. Zhang, and T. Kuang, “Selective laser melting of high-performance pure tungsten: parameter design, densification behavior and mechanical properties,” *Sci Technol Adv Mater*, vol. 19, no. 1, pp. 370–380, 2018, doi: 10.1080/14686996.2018.1455154.

[7] Van Staden, A. C., et al. 2016. “Characteristics of single layer selective laser melted toolgrade cemented tungsten carbide. In Competitive Manufacturing”, *International Conference on Competitive Manufacturing (COMA '16)*, 27-29 January 2016, Stellenbosch, Stellenbosch University, South Africa.

[8] E. Broitman, “Indentation Hardness Measurements at Macro-, Micro-, and Nanoscale: A Critical Overview,” *Tribol. Lett.*, vol. 65, no. 1, pp. 1–18, 2017, doi: 10.1007/s11249-016-0805-5.

[9] Shen, Xianfeng, et al. “Effect of Substrate on Temperature Field in Selective Laser Sintering of Metal Powders.” *International Congress on Applications of Lasers & Electro-Optics*, 2009, doi:10.2351/1.5061650.

[10] AISI Type H13 Hot Work Tool Steel, www.matweb.com/search/datasheet_print.aspx?matguid=e30d1d1038164808a85cf7ba6aa87ef7

[11] Stuart, R. V. *Vacuum Technology, Thin Films, and Sputtering: An Introduction*, Elsevier Science (2012)

[12] S. Kumar and U. Batra, “Surface modification of die steel materials by EDM method using tungsten powder-mixed dielectric,” *J. Manuf. Process.*, vol. 14, no. 1, pp. 35–40, 2012, doi: 10.1016/j.jmapro.2011.09.002.

[13] G. Lumay *et al.*, “Measuring the flowing properties of powders and grains,” *Powder Technol.*, vol. 224, pp. 19–27, 2012, doi: 10.1016/j.powtec.2012.02.015.

[14] N. Ku, J. J. Pittari, S. Kilczewski, and A. Kudzal, “Additive Manufacturing of Cemented Tungsten Carbide with a Cobalt-Free Alloy Binder by Selective Laser

[15] A. Tyurin, S. Nagavkin, A. Malikov, and A. Orishich, “Microstructure of WC–Co hard alloy surface after laser treatment,” *Surf. Eng.*, vol. 31, no. 1, pp. 74–77, 2014, doi: 10.1179/1743294414y.0000000398.Melting for High-Hardness Applications,” *Jom*, vol. 71, no. 4, pp. 1535–1542, 2019, doi: 10.1007/s11837-019-03366-2.